2022

THERMAL PROPERTIES OF WATER REPELLENT SANDS: EXPERIMENTAL AND THEORETICAL EVALUATION

Gang Lei

THERMAL PROPERTIES OF WATER REPELLENT SANDS: EXPERIMENTAL AND THEORETICAL EVALUATION

by

Gang Lei

Presented to the Faculty of the Graduate School of

The University of Texas at Arlington

in Partial Fulfillment of the Requirements

for the Degree of

DOCTOR OF PHILOSOPHY

THE UNIVERSITY OF TEXAS AT ARLINGTON

August 2022

This work is dedicated to my beloved parents.

ACKNOWLEDGEMENT

It is my pleasure to express gratitude to my advisor Dr. Xinbao Yu, and co-advisor Dr. Laureano Hoyos for their guidance, support, and generosity. It was a great fortune to meet them and to work with them making my Ph.D. experience at the University of Texas at Arlington.

I would like to thank the members of my committee, Dr. Nick Fang, and Dr. Qinhong (Max) Hu, for their invaluable feedback and encouragement. I would also like to thank Dr. Haiying Huang, Dr. Jiechao Jiang, Dr. Aritra Banerjee, and Dr. Tejo V. Bheemasetti for sharing with me their experience and extensive knowledge through their courses of study and laboratory works.

I am also thankful to my colleagues in Dr. Yu's research group throughout the years we worked together. I offer sincere thanks to Dr. Xuelin Wang, Nice Kaneza, Dr. Shi He, Dr. Liyang Wang, Dr. Teng Li, Sandesh Gautam, Dr. Omid Habibzadeh, Taryn Dilorenzo, Arjan Poudel, Mehran Azizian, Hussein Hashemi Senejani, and Natnael Asfaw for their friendship and support and for providing a dedicated working environment. Special thanks to my dear friend, Xiaoqing Yuan, for her prominent help, encouragement, and heartfelt compliments.

Finally, I genuinely thank my family for their uninterrupted and incomparable help, love, and support. I am forever grateful to my parents for giving

me the opportunities and experiences that have made me who I am. They altruistically encouraged me to discover new directions in life and seek my destiny. This journey would not be possible without them, and I dedicate this dissertation to my parents.

July, 2022

TABLE OF CONTENTS

LIST OF ILLUSTRATIONS

LIST OF TABLES

ABSTRACT

THERMAL PROPERTIES OF WATER REPELLENT SANDS: EXPERIMENTAL AND THEORETICAL EVALUATION

Gang Lei

The University of Texas at Arlington, 2022

Supervising Professor: Dr. Xinbao Yu and Dr. Laureano Hoyos

Unsaturated hydrophobic soils, induced by the decomposition of plant roots or chemical or oil contamination et al., may have potentially negative effects on soil thermal behaviors and further influence the performance of shallowly buried energy systems, including ground heat exchangers, borehole energy geo-storage systems, and buried power cable systems, etc. This research focused on the fundamental understanding of soil thermal behaviors in relation to surface wettability.

Surface wettability alteration was conducted in the laboratory by applying dimethyldichlorosilane (DMDCS) on dry sands, which generated a thin hydrophobic layer on the sand particle surface. Several surface characterizations using scanning electron microscopy (SEM), energy dispersive spectroscopy (EDS), and Raman Microscopy, were performed to verify the surface modification. The generated polydimethylsiloxane (PDMS) on the sand surface has been proved to be strong bonding.

Laboratory experiments were conducted on two types of quartz sands with various water repellencies using the KD2 standard probe to investigate the effects of level of water repellency, porosity, degree of saturation, and temperature on soil thermal conductivity. The water repellency was found to mitigate soil thermal conductivity by hindering the formation of water bridges at the particle contacts. Nonuniform water distribution within soils was induced, therefore resulting in poor pore fluid connectivity and further generating deficient paths of heat conduction.

Based on the experimental results on Ottawa 20/30 and 50/70 sand with various degrees of water repellency, a continuum soil thermal conductivity prediction model was developed. The model overcame the shortcomings of the existing models, accounting for the hydrophobization effect. Validation was performed that the predicted thermal conductivities were found to be in good agreement with experimental data. When estimating thermal conductivity with full range of degree of saturation, the new continuum thermal conductivity prediction model needs parameter calibration.

CHAPTER 1. INTRODUCTION

1.1. Background

Over the past few years, tremendous engineering applications have been conducted in which soils are subjected to thermal load. Examples of these applications include geothermal systems especially ground heat exchangers (Laloui and Rotta Loria, 2019), buried power cable systems (Boggs, 1982), energy geo-storage systems (Stauffer et al., 2013), and nuclear waste storage and repositories (Ojovan et al., 2019). Many new energy-related projects are planned and/or under development in many regions, where the groundwater table is often deep, and soils are unsaturated. In most cases, geo-exchange systems such as ground heat exchangers and energy geo-storage systems depend on the vadose zone, namely the unsaturated zone, to provide a large percentage of the geo-heat sink (Houston et al., 2015). During the operation of energy conversion systems such as ground heat exchangers, heat is retracted from the ground for heating infrastructures and injected into the ground as heat storage during summer times. This induces thermal gradients among adjacent soils. The gradient results in moisture transfer within unsaturated soils and this transport in return affect the heat flow. Additionally, the surface property of soils determines the wetting behaviors of the pore fluid in

unsaturated soils, and further, the soil-water interaction and the liquid-air distribution dominate the mechanical property of soils (Dong, 2013). Enormous studies have been conducted to investigate the thermal, hydraulic, and mechanical behaviors, as well as their coupled effects, of unsaturated soils. However, all studies were performed with the assumption of soil as a hydrophilic material. In nature, water repellent soils are widespread, and soil hydrophobicity stems from mineral-associated soil organic matter (Doerr et al., 2000), plant species (Franco et al., 2000), contaminants (Selker et al., 1991), and wildfires (Shakesby and Doerr, 2006) et al.. Soil water repellency (SWR) has substantial hydrological repercussions from reduced soil infiltration and enhanced surface runoff to the development of preferential flow (Ritsema and Dekker, 1996). Since the SWR influences the distribution of water in soils and water distribution affects some of the thermal properties, water repellency may impact some of the thermal properties of soils. Furthermore, some of the aforementioned energy systems, for example, buried power cable systems, are shallowly buried. The adjacent soils might have some extent of hydrophobicity due to the decomposition of plant roots or chemical or oil contamination, modifying original soil surfaces and then influencing soil thermal, hydraulic, and even mechanical properties. Therefore, it's necessary to expand the understanding of conduction (thermal and hydraulic conductions) behaviors of unsaturated water repellent soils.

1.2. Motivation and Objectives

The current research mainly focuses on the evaluation of hydrological and erosional behaviors of water repellent soils, including hydraulic conductivity and degradation under weathering conditions such as wetting-drying and high temperature. Potential engineering applications of hydrophobic soils as impermeable barriers for slope protection have also been investigated in the laboratory. In terms of thermal behaviors of soils, current investigations of thermal properties have assumed that soils are hydrophilic materials. In nature, soils are with some extent of water repellency, especially soils affected by plant roots or contaminations. Limited research has investigated the thermal response of soils with various wettability. A knowledge gap remains in terms of overall evaluations of thermal behaviors of hydrophobic soils over the entire saturation range and related thermal conductivity prediction models. This study attempts to fill this gap utilizing experimental investigations, followed by detailed analysis and discussion. Based on the previous studies, the problem statements in this study are summarized as follows,

1. Lack of investigations of effects of water repellency on backfill materials in the energy application field,

2. Insufficiency of a systematic and comprehensive evaluation of water repellency induced changes in soil thermal properties,
3. Absence of thermal conductivity prediction models for hydrophobic soils.

Accordingly, the specific research objectives in this study are listed below,

1. To perform hydrophobic coating on the soil surface and conduct surface characterizations,
2. To evaluate the effects of soi hydrophobicity on soil thermal properties,
3. To develop a new continuum soil thermal conductivity model considering soil hydrophobicity.

1.3 Dissertation Structure

The subsequent chapters of this thesis are organized as follows:

Chapter 2 presents an extensive review of the fundamentals of soil wettability, including theoretical models, origins, and quantification methods. The influences of soil water repellency on thermal and hydraulic properties are summarized, and existing soil thermal conductivity prediction models are introduced.

Chapter 3 reports the hydrophilization of two granular materials (Ottawa 20/30 and 50/70 sand) using the hydrophobizing agent (Dimethyldichlorosilane). Contact angles and characterization of the modified sand surface were conducted to verify the particle coating.

Chapter 4 centers on the thermal behavior of sands in both hydrophilic and hydrophobic status based on laboratory experiments. The effect of the degree of water repellency on sand thermal conductivity was investigated.

Chapter 5 documents the development of a new continuum soil thermal conductivity model based on the experimental data presented in Chapter 4. This model was proposed based on Campbell's (1994) model, which accounts for changes both in the degree of saturation and temperature.

Chapter 6 summarizes general key conclusions and offers recommendations for future studies.

CHAPTER 2. LITERATURE REVIEW

2.1. Introduction

This chapter provides literature reviews on the fundamentals and background of soil wettability and existing soi thermal conductivity prediction models. It is divided into three subsections, namely, soil hydrophobicity, influence of water repellency, and soil thermal conductivity prediction models. The principles of wetting are first introduced, followed by the origins of soil repellency and quantification methods of soil hydrophobicity. Then, the influence of water repellency on soil thermal and hydraulic properties is detailed discussed. Finally, the existing soil thermal conductivity prediction models are summarized and categorized into three groups, viz. theoretical models, empirical models, and other models.

2.2. Soil Hydrophobicity

2.2.1. Principles of wetting

Wetting of a solid by a liquid stem from a relatively high degree of attraction between the molecules of solid and liquid. This attraction of the molecules of the liquid determines the extent of wetting, namely wettability, of a solid surface (Bornemisza, 1964). In natural soils, wettability affects many processes such as infiltration (Lourenço et al., 2018). The wettability of solids is generally expressed by their contact angle (CA). When a drop of liquid is placed on a dry and flat solid surface, it becomes equilibrium forming a three-phase contact line between the solid, liquid, and gas (Figure 2-1). When the water drop reaches equilibrium, the interfacial tensions acting at the interfaces, namely the solid-air (γ_{sa}), solid-liquid (γ_{sl}), and liquid-air (γ_{la}), must balance. This equilibrium relation between surface tensions and contact angles has been recognized by Young (Young, 1805). And the relation is known as Young's equation:

$$\gamma_{la} cos\theta_y = \gamma_{sa} - \gamma_{sl} \quad (2.1)$$

Where, θ_y is the Young contact angle. The wettable solid surfaces have contact angles <90º and the wetting process occurs instantaneously at an angle of 0º, while materials with contact angles >90º are defined as water-repellent. Usually,

contact angles just lower than 90º are called ‘sub-critical water repellency (Bornemisza, 1964).

Young’s equation is valid on an ideal solid surface, namely, the surface is smooth, flat, homogenous, inert, non-porous, and non-deformable (D. Y. Kwok et al., 1997). However, in practice, due to the roughness and heterogeneity of solid surfaces, the measured contact angles become apparent. Besides, contact angle hysteresis occurs resulting from non-identical advancing and receding contact angles made by advancing and receding liquids, respectively (D.Y.Kwok and A.W. Neumann, 1999). The value of the apparent contact angle falls between the advancing and receding contact angles (Lourenço et al., 2018). The deviation of θ_a from θ_y (Young’s CA) stems from the contamination of solid surfaces and liquids and solid surface roughness (D. Y. Kwok et al., 1997).

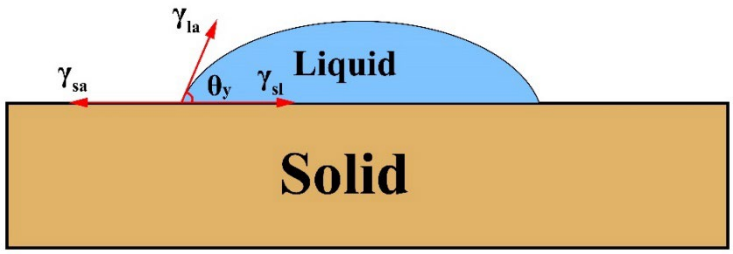

Figure 2- 1. Interfacial equilibrium of a water drop on a flat surface.

The aforementioned principles of wetting are applicable to smooth surfaces rather than rough surfaces. Studies on the effects of surface roughness on wetting

have been carried out by Wenzel (Wenzel, 1936) and Cassie and Baxter (Cassie and Baxter, 1944). Wenzel recognized the difference between the total or 'actual surface' of an interface and its superficial or 'geometric surface' which is the surface as measured in the plane of the interface. Then the concept of surface roughness, which results in the distinction between actual surface and geometric surface at the surface of real solids, was proposed and integrated into an equation in relation to liquid drop contact angle (Wenzel, 1936). The equation can be written as (Blossey, 2003):

$$rcos\theta_y = cos\theta_w \tag{2.2}$$

where r is the surface roughness factor, known as the ratio of the actual surface of a solid surface to its geometric surface; θ_y is the intrinsic angle or Young's contact angle; θ_w is the Wenzel apparent contact angle (WCA), indicating the apparent contact angle affected by the roughness of a solid surface. Eq. (2.2) is related to the homogeneous wetting regime, described by Wenzel, that when spreading on a real solid surface (rough), water will fully penetrate the rough grooves (Marmur, 2003), as shown in Figure 2-2(a). Therefore, the equation also indicates that for hydrophilic surfaces, the WCA decreased as surface roughness increased, which was also observed by AlRatrout et al. (2018). On contrary, the θ_w on hydrophobic surfaces became higher as the surface roughness increased (Wenzel, 1936).

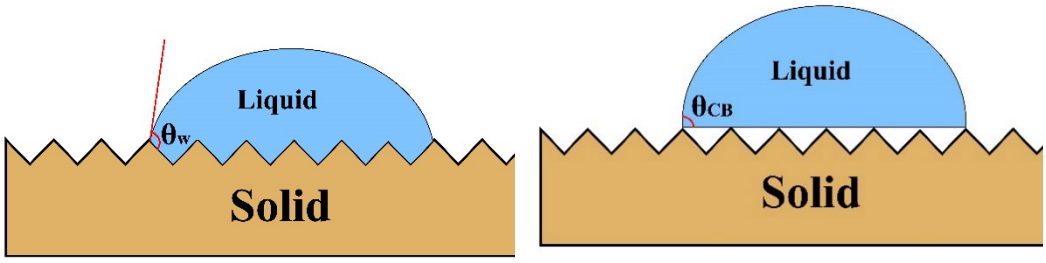

(a) (b)

Figure 2- 2. Schematic presentation of contact angles on solid surfaces: (a) Wenzel state (homogeneous); (c) Cassie-Baxter state (heterogeneous).

Cassie and Baxter (1945) extended the Wenzel equation to porous surfaces and to surfaces rough enough that air can be entrapped at the interface between the solid and the water, as shown in Figure 2-2(b). In the Cassie-Baxter wetting state (heterogeneous), contacts between the liquid and solid only occur through asperities. An equation has been developed for the apparent contact angle for porous surfaces (Cassie and Baxter, 1944):

$$cos\theta_{CB} = f_1\theta_y - f_2 \tag{2.3}$$

where θ_{CB} is the Cassie-Baxter (CB) apparent contact angle; θ_y is the intrinsic contact angle or Young's contact angle; f_1 the total area of solid-water interface; and f_2 is the total area of the air-liquid interface per unit superficial area of the interface. When the surface is rough but not porous, f_2 in Eq. (2.3) is zero, and the CB equation turns into Wenzel's equation.

The CB wetting states occur on a heterogeneous surface formed by two homogeneous surfaces of the respective materials (Blossey, 2003). From the CB equation, by weighting the amount of each available homogeneous surface, one can determine the apparent contact angle of a liquid drop on the heterogeneous surface by summing the cosines of the contact angles on two homogeneous surfaces. If one of the surfaces is just air, the cosine of the contact angle on the air surface is -1, then the CB equation can be written as another form (Blossey, 2003) :

$$cos\theta_{CB} = -1 + \phi_s(1 + cos\theta_y) \tag{2.4}$$

where ϕ_s is the fraction of the solid. When ϕ_s tends to be zero, the apparent contact angle will tend to 180º, meaning that liquid drops will lift off the solid surface. Johnson and Dettre (1964) demonstrated this mechanism mathematically for an idealized sinusoidal surface and concluded above a certain value of the surface ratio, the CB contact angle is about to reach an equilibrium state. If we consider the ratio of the actual wetted area to the projected area, Eq. (2.4) can be written as (Gao and Yan, 2009; Marmur, 2003; Wang et al., 2020):

$$cos\theta_{CB} = r\phi cos\theta_y + \phi - 1 \tag{2.5}$$

where $\phi \in [0,1]$ is the fraction of the projected area of the liquid-solid interface; r is the surface roughness ratio. When ϕ equals 1, meaning that the whole projected area is wetted by liquid, this equation turns to the Wenzel equation.

2.2.2. Origins of soil water repellency

Soil water repellency (SWR) is rarely due to the hydrophilic soil components but to some external factors such as naturally occurring waxes, fungi, and organic matters resulting from contaminations and wildfires et al., and artificial coating on soil particle surfaces using chemicals or polymers (Bourrié, G. (Ed.), 2019; Lourenço et al., 2018). For example, sand, composed of silica, is expected to be wettable and has a wettability relatively close to that of glass associated with a small contact angle. But, if sand is extremely dry, it may behave like hydrophobic materials, as shown in Figure 2-3. It is commonly accepted that the main factor inducing soil hydrophobicity is the deposit of organic compounds stemming from decomposing plants or microorganisms (Ma'shum et al., 1988). However, the natural abundance of various, potentially responsible substances results in difficulties in identifying the exact substance(s) responsible for causing water repellency in a given soil (Doerr et al., 2000). For instance, 93 organic compounds, of which many were water repellent, were extracted from just one sampled soil by Almendros et al. (1988).

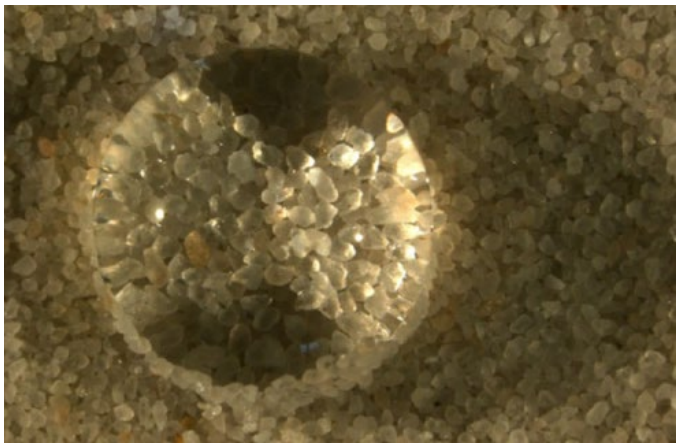

Figure 2- 3. Hydrophobic behavior of extremely dry soils: single water drop resting on medium-size sand surfaces (Lourenço et al., 2018).

The organic compounds extracted from natural hydrophobic soils can be split into two groups. The first is the aliphatic hydrocarbons, which are non-polar and almost insoluble in water, comprising hydrogen and carbon with carbon atoms arranged in an elongated chain (Doerr et al., 2000). The second group contains polar substances with an amphiphilic structure, consisting of both a hydrophilic part (polar) and a hydrophobic part (non-polar) (Figure 2-4(I)). Several conceptual models in terms of interaction mechanisms between amphiphilic molecules and mineral surfaces have been developed as shown in Figure 2-4(II/a-c). The polar functional group of amphiphilic molecules is more attractive to silicate soil particles due to hydrogen bond and/or dipole interactions, leaving the non-polar chain exposed (Mainwaring et al., 2013; Ma'shum et al., 1988). Additionally, the non-polar chain of amphiphilic compounds behaves in weak interactions with the soil

surface and any incoming water through van der Waals forces (Daniel et al., 2019). Therefore, the dipole interaction between the hydrophilic end of amphiphilic molecules and the polar soil surface is expected to be maximized and results in the formation of a hydrophobic barrier since the hydrophobic chains will be toward the outside (Bourrié, G. (Ed.), 2019; Doerr et al., 2000).

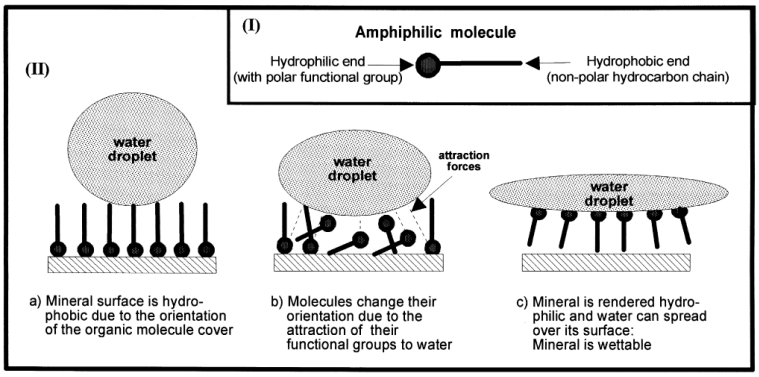

Figure 2- 4. Schematic diagram of (I) an amphiphilic molecule and (II/a-c) contact between a mineral surface and water droplet with changes in orientation of the molecules (Doerr et al., 2000).

As aforementioned, a hydrophilic mineral surface can be rendered as a hydrophobic surface by one monolayer of hydrophobic molecules (Zisman, 1964). This provides approaches to artificialize synthetic water-repellent soils (SWRS) in the laboratory, which can be used as barriers to infiltration or materials for ground improvement, by coating hydrophobic compounds on soil surfaces (Dong, 2013; Ma'shum et al., 1988). During the last decade, researchers have investigated the

feasibility of applying synthetic water-repellent soils as alternatives to improve the performance of landfill cover systems (Dell'Avanzi et al., 2010; Zheng et al., 2021). Hydrophobic soils have been approved to be functional as landfill covers in arid areas but not in tropical or subtropical regions (Dell'Avanzi et al., 2010). Zheng et al. (2021) further analyzed the performance of capillary barriers comprised of water-repellent soils in tropical climates by conducting laboratory model tests in an inclined flume. Artificial rainfalls were applied to simulate tropical climates. Their results revealed that the barrier effect was significantly strengthened, and the construction cost can be decreased by using synthetic hydrophobic soils. Furthermore, SWRS with reversible surface wettability has been manipulated by coating temperature-susceptible polymers on sand surfaces (Dong, 2013). This type of engineered soil is more durable to adjust the behavior of engineered facilities to adapt to environmental changes.

2.2.3. Measurements of soil hydrophobicity

To assess soil water repellency, both qualitative and quantitative methods have been developed and applied in soil science. Qualitative measurements, of which set-ups are simple, are generally used in the field and developed as index tests. Usually, quantitative methods require special equipment and are performed in the laboratory to obtain parameters including contact angles, surface tensions,

and water entry pressures of hydrophobic soils. Detailed measurement methods are summarized in Table 2-1.

Table 2- 1. Summary of soil hydrophobicity measurement methods (Lourenço et al., 2018).

Methods	**Sample conditions**	**Setting**	**Characteristic**	**Parameter, unit**
Sessile drop method	Monolayer of soils	In lab	Quantitative	Static CA, degree
Water drop penetration time test	Bulk soils	In lab and in-situ	Qualitative	Time, seconds
Molarity of ethanol drops test	Bulk soils	In lab and in-situ	Qualitative	Surface tension, nN/m
Capillary rise method	Bulk soils	In Lab	Quantitative	Advancing CA, degree
Water entry pressure test	Bulk soils	In lab	Quantitative	Water heat, cm
Wilhelmy plate method	Monolayer of soils	In lab	Quantitative	Advancing and receding CA, degree

2.2.3.1. Sessile drop method

The sessile drop method (SDM) is a direct method to measure the apparent CA of a water drop on a smooth surface. Bachmann et al. (2000) modified the method and made it suitable for measuring the CA of soil particles. The assumptions of this method for soil contact angle measurements are that gravitational effects on the drops are negligible and the heterogeneity is limited, meaning that soil samples are sieved particles of the same size. The procedures of SDM are as follows: (1) placing soils on a double-sided adhesive tape on a glass

slide, and a small pressure is applied to ensure a monolayer of soil particles is fixed and any motion of the particles is avoided, followed by gently shaking the glass slide to remove the excess particles. (2) placing the soils with a glass slide on a goniometer's stage and dispensing a pre-determined volume of a deionized water droplet on the sample. The volume of drop usually ranges from 1 to 2 µl (Lourenço et al., 2018) but drop volumes up to 20 µl can be also adopted (Buczko and Bens, 2006). (3) Recording the water droplet on the soil monolayer and measuring CA by fitting the outline of droplet and baseline, as shown in Figure 2-5.

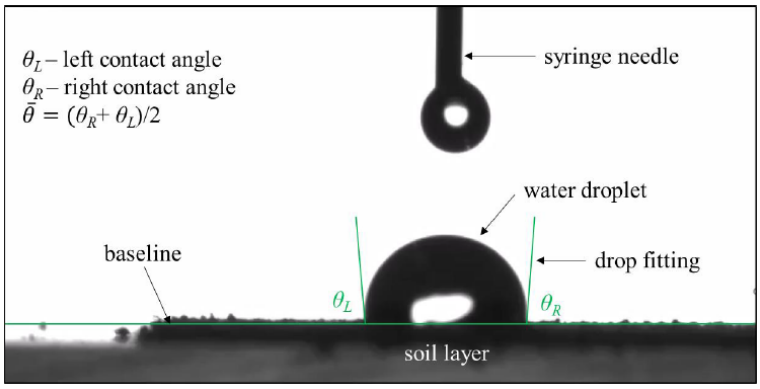

Figure 2- 5. The contact angle (CA) measurement via the sessile drop method on a soil monolayer (Lin, 2020).

Improvements of SDM have been performed by Saulick et al. (2017) to mitigate the standard deviation of CA determination. The authors examined the steps involved in determining the CA on granular materials, such as soils, and showed that two factors, the image exposure and the position of the baseline, can

significantly affect CA measurements. A semi-automated technique was then proposed with five steps, which can manually adjust the image exposure and movement of the baseline. This semi-automated technique improved the standard deviation of measurements of CA by 33% on granular materials.

2.2.3.2. Water drop penetration time test

Water drop penetration time is an index to assess the persistency of soil hydrophobicity. It has been widely used in the laboratory and field because of its simple and quick operation. The WDPT test measures the time needed for a water droplet to fully penetrate the soil. Classification of soil water repellency persistence was proposed based on the WDPTs ranging from wettable (<5s) to extremely hydrophobic (>3600s) (Doerr, 1998). This hydrophobicity classification is summarized in Table 2-2. In this study, 5-15 drops of distilled water with volumes typically varying between 50 and 80 μL are placed on a soil surface (Figure 2-6). Then the time for the penetration of the water droplet is recorded. The samples are covered with lids to prevent evaporation to allow the test to be extended to over 5h. Finally, the recorded time is compared with the hydrophobicity classification.

Table 2- 2. Levels of water repellency and corresponding WDPT (Doerr, 1998).

Water repellency level	WDPT (s)
Wettable	≤ 5s
Slightly water repellent	5-60s
Strongly water repellent	60-600s
Severely water repellent	600-3600s
Extremely water repellent	≥3600s

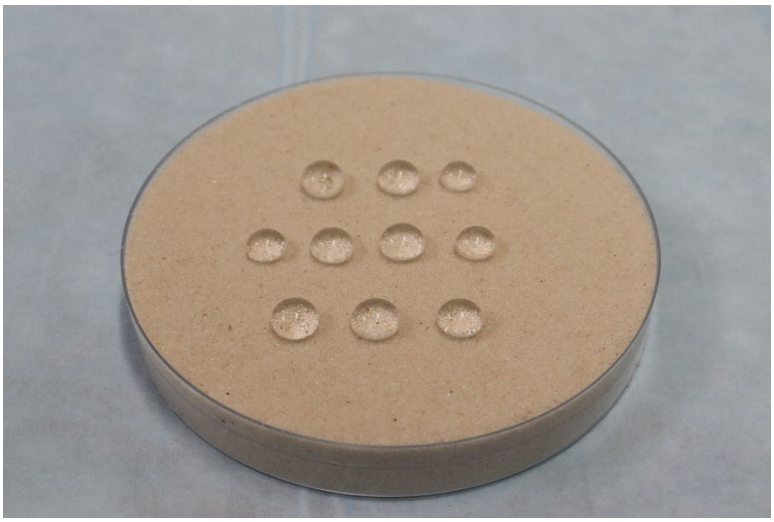

Figure 2- 6. WDPT test on hydrophobic soil.

2.2.3.3. Molarity of ethanol drops test

Originally proposed by King (King, 1981), the molarity of an ethanol drop (MED) test is a useful method for evaluating water repellency since it's more rapid than WPDT and easily performed in the laboratory or field on soil surfaces (Dekker et al., 1998; Kawamoto et al., 2007). This method has similar procedures to WDPT (Moody and Schlossberg, 2010). Ethanol droplets with various concentrations are

dispensed on soil surfaces. The MED test quantifies water repellency as the lowest ethanol concentration permitting droplet infiltration into soils within 5 s (Moody and Schlossberg, 2010). Additionally, the water repellency can be quantified by the 90º liquid surface tension of the infiltrating droplet. However, even using the solid-vapor tension to quantify water repellency (Gilboa et al., 2006), the MED test poorly represents soil wetting behavior (Doerr and Thomas, 2000).

2.2.3.4. Capillary rise method

The wettability of soils is generally assessed by the penetration time of a known volume of water (water penetration test) or by the rate of movement of the wetting front into dry soils (capillary rise method) (Bornemisza, 1964). The water drop penetration test was detailed and reviewed in Section 2.2.3.2. Both methods are influenced by gravity, hydrostatic pressure, pore size distribution, and the physical and chemical properties (i.e., contact angle) of the soil surfaces. The first two factors are not considered in this review. The effects of pore size distribution and contact angle have been investigated decades ago based on Poiseuille's equation. Washburn (1921) integrates this equation to describe capillary absorption based on the assumption that porous materials behave as an assemblage of small cylindrical tubes when liquid penetrates a porous body. The contact angle can be back-calculated using the simplified Washburn equation (Washburn, 1921):

$$h^2 = \frac{r\gamma_l cos\theta}{2\eta} t \quad (2.6)$$

where h (m) is the height of the liquid front rising in the column; r (m) is the effective radius of the uniform pores of the granular material; γ_l (J/m^2) is the surface tension of the liquid; θ is the contact angle of the bulk sample; η (Pa·s) is the viscosity of the liquid, and t (s) is the time.

The capillary rise method (CRM) has been vastly implemented in measuring contact angles for soils. Furthermore, analytical solutions to various forms of the Washburn equation have been studied to apply CRM to soils. However, the application of CRM is limited to hydrophilic soils and is not suitable for hydrophobic soils.

2.2.3.5. Water entry pressure test

Water entry pressure (WEP) is the critical pressure at which water starts to penetrate the soil pores (Feyyisa et al., 2019). It acts as one of the important indicators of soil water potential, which also can be treated as an indicator of soil wettability. For wettable soils, the WEP is negative due to negative soil water potentials; while water-repellent soils were found to have positive WEPs (Figure 2-7) (Wang et al., 1998). In addition, a number of laboratory tests investigated the variations of the water entry pressure of soils concerning various porosities. Among those tests, two methods have been mainly utilized for WEP measurements. The

water-ponding (WP) method, which is widely used, is to directly apply a water head on the soil surface and increase the water head util infiltration occurs (Carrillo et al., 1999). This method is limited to hydrophobic soils. The other method, tension-pressure infiltrometer (TPI), can assess the wettability of hydrophilic and hydrophobic soil using WEP (Wang et al., 2000). The TPI stems from the tension infiltrometer and can supply water pressure starting from zero. Lee et al. (2015) examined the hydraulic behavior of an artificial water repellent silty soil treated with an organo-silane solution based on TPI and found that a unique range of porosity values was produced by the treatment with four chemical concentrations. The water entry pressure increased with decreasing porosity and increasing concentration.

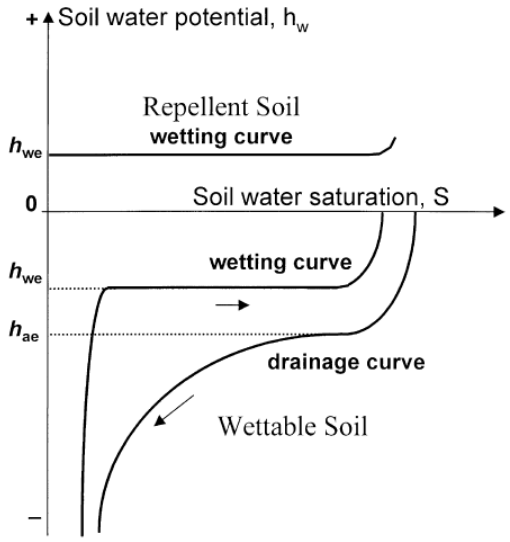

Figure 2- 7. Soil water retention curves for a wettable and repellent soil (the h_we and h_ae denote water entry and air entry values of the porous soils, respectively) (Wang et al., 2000).

2.2.3.6. Wilhelmy plate method

The Wilhelmy plate method has been utilized over the entire range of dynamic contact angles (Ramé, 1997). This technique partially immerses a plate with a thickness much smaller than the other dimensions vertically into a fluid. The plate is hung by a balance. From the reading of the balance, the vertical component of the force acting on the plate is measured. The total force F_t acting on the plate is presented as (Bachmann et al., 2003)

$$F_t = W - F_b + F_W = W - V\rho g + l_w\gamma_{la}cos(\theta) \quad (2.7)$$

where W is the weight of the plate, F_b is the buoyancy force, F_W is the wetting force, V is the volume of the sample that is immersed, ρ is the density of the fluid, g is the gravitational constant, l_w is the wetted length of the sample, γ_{la} is the liquid-air surface tension, and θ is the contact angle. If the balance is tared, the contact angle can be calculated as

$$cos(\theta) = \frac{(F_t + V\rho g)}{l_w \gamma_{la}} \tag{2.8}$$

This technique was firstly proposed by Bachmann et al. (2003) for granular materials. A glass plate with double-side tape on each side is utilized for the test. A one-grain layer of soil particles covers the adhesive tapes. Then, the glass plate is attached to an electronic balance hanging vertically and gradually immersed in water as shown in Figure 2-8. The contact angle can be obtained using Eq. (2.8).

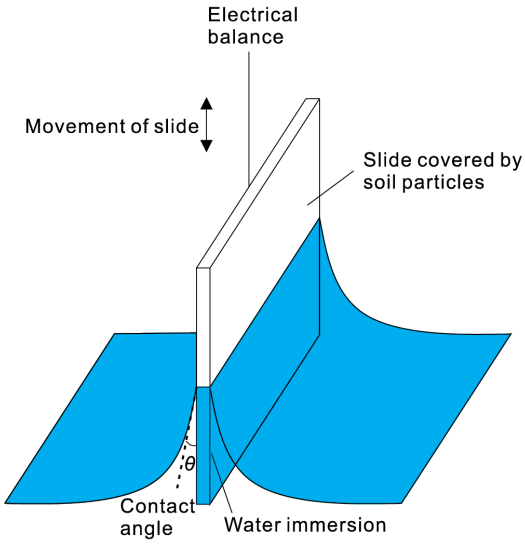

Figure 2- 8. Schematic representation of the set-up of WPM.

2.3. Influence of Soil Water Repellency on Thermal Properties

The study of soil thermal properties, including thermal conductivity, diffusivity, and heat capacity, is critical in various energy-related applications such as geothermal heat exchangers, buried power cables, and energy piles. For example, boreholes and energy piles connected to ground-source heat pumps (GSHP) are utilized to extract and inject geothermal energy for heating and cooling bridges and buildings. The extraction/injection efficiency is mainly subjected to the temperature and moisture changes among thermal interfaces between pile/borehole and surrounding soil, especially in the soil layer above the water table (Fadejev et al., 2017; Xiao and Suleiman, 2015). Also, the electric current rating for buried cable depends on the thermal conductivity of the surrounding soil (Brandon et al., 1989). Several physical factors that influence thermal responses of soils have been studied, such as moisture content, dry density, mineral components, soil particle gradation, grain shape, and pore fluid (Abu-Hamdeh, 2003; Farouki, 1981; Li et al., 2020; Oh and Tinjum, 2021; Zhang et al., 2017b). Among these, the water content plays a major role. For instance, soil thermal conductivity, a vital parameter that determines the temperature distribution in soils (Zhang et al., 2017b), usually increases as moisture content rises (Yu et al., 2016). However, the surface wettability of soils has not been considered in almost all studies in terms of soil thermal properties.

Limited research has investigated the thermal response of soils with various wettability. Dong (2013) continuously measured the evolution of thermal conductivity of both regular (hydrophilic) and polymer-coated (hydrophobic) sands versus the degree of saturation. The thermal conductivity of hydrophobic sands is much lower than that of hydrophilic sands except when the degree of saturation is above ~80%. This phenomenon doesn't match what was observed by Bachmann (2001) and Ju (2008). Although they also found that the thermal conductivity of water-repellent soils decreases compared to hydrophilic soils, the magnitude of the reduction is much less than that obtained in Dong's study. The deviation might attribute to different types of coating agents and soil types since both Bachmann and Ju treated soils using dimethyldichlorosilane (DMDCS) but not polymers. Aside from the difference, the de Vries model (Vries and Philip, 1986) was involved in both Dong's and Bachmann's studies. The predicted thermal conductivity by mixture models (DeVera and Strieder, 1977) in Dong's research is superimposed to delineate upper and lower bounds for measured data. And Bachmann's research directly applied the de Vries model to predict thermal conductivities with magnitudes less than measured thermal conductivities. But this result differs from previous studies in that the measured conductivities were generally less than those predicted by the model (Horton and Wiernga, 1984; Kimball et al., 1976). Due to several contradictions that occurred in previous studies, the thermal properties of water repellent soils, especially thermal conductivity, need

a deeper and more sophisticated investigation. More efforts also have to be taken to develop a new thermal conductivity prediction model for water repellent soils with higher accuracy compared with current models.

2.4. Soil Thermal Conductivity Prediction Models

Since soil thermal conductivity acts as one of the key factors in the design of geothermal-related structures such as borehole thermal energy stores (BTES), etc., accurate prediction of soil thermal conductivity is urgently needed. A bunch of experimental studies has been carried out by researchers to investigate soil thermal properties, and the results attributed the three main influencing factors of soil thermal conductivity to moisture content, dry density, and soil mineral components. The existing models also selected these three factors as variables for predicting soil thermal conductivity.

Both Dong et al. (2015) and Zhang et al. (2017) summarized critical reviews of soil thermal conductivity and predictive models. They divided soil thermal conductivity models into three categories, namely, empirical models, theoretical models, and other models. This section presents the review of the origin and several existing soil thermal conductivity models, which have been widely applied to soil science and geotechnical engineering.

2.4.1. Theoretical models

2.4.1.1. Wiener model

The concept of upper and lower limits of the thermal conductivity of the porous medium, including solid, liquid, and gas, was firstly introduced by Wiener (1912). The effective thermal conductivity of porous medium is based on classical mixing laws (arithmetic and harmonic) of series model and parallel model, which are expressed as,

$$k_{eff} = \left[\sum_{i=1}^{3} \phi_i \cdot \frac{1}{k_i}\right]^{-1} \quad \text{(series)} \tag{2.9}$$

$$k_{eff} = [\sum_{i=1}^{3} \phi_i \cdot k_i] \quad \text{(parallel)} \tag{2.10}$$

where ϕ_i is the volume fraction of each phase (i can be a (air), w (water), s (solid)), k_i (W/m·K) is the thermal conductivity of each phase ($k_a = 0.56, k_w = 0.026$).

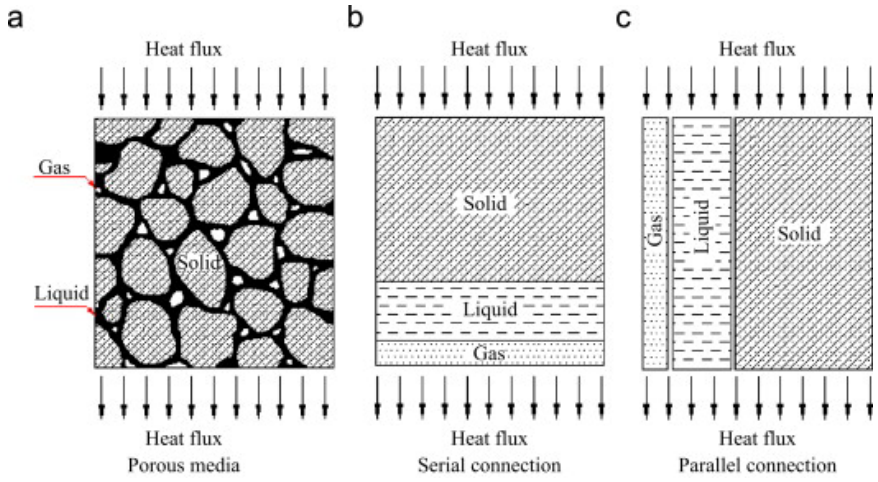

Figure 2- 9. Schematic illustration of the series and parallel models corresponding to Wiener lower and upper bounds, respectively (Tong et al., 2009).

Figure 2-9 presents the schematics of Wiener bounds of thermal conductivity of porous media. The series model, lower Wiener bound, applies a constant heat flux through each serially connected component (Figure 2-9b), where the temperature gradient corresponding to each component is determined by its thermal conductivity. While the parallel model imposes an identical temperature gradient within each phase/element (Figure 2-9c). In this case, each phase has the same temperature difference, but different heat flows due to its dependence on the thermal conductivity of each element. The Wiener model is the most classic one and forms the foundation of heat conduction in porous media for other common theoretical models. It has been widely modified to develop thermal conductivity models for soils under different scenarios.

2.4.1.2. De Vries model

De Vries' method (1963) originated from Maxwell's equation for the electrical conductivity of a mixture of uniform spheres dispersed randomly in a continuous fluid. This was later utilized to predict the thermal conductivity of soils in a continuous medium of air or water. The assumptions of the De Vries equation are that particles are not in contact, which is not suitable for soil. In addition, the g values, namely, particle shape factors, assumed by De Vries indicate a needle-like shape, differing from most soil particles. To apply the method to moist, unsaturated soils, another assumption was added that the solid particles and the air voids are considered to be two components dispersed in the continuous water medium. This assumption needs the water content of soil surpasses a certain minimum so that the water medium may still be regarded as continuous. The thermal conductivity of the unsaturated soil is given by

$$k_{eff} = \frac{\phi_w k_w + F_s \phi_s k_s + F_a \phi_s k_a}{\phi_w + F_s \phi_s + F_a \phi_s} \tag{2.11}$$

where F_i and ϕ_i are weight and volume fraction of each phase, respectively. Factor F is given by

$$F_s = \frac{1}{3}\left\{\frac{2}{1 + [(k_s/k_w) - 1]0.125} + \frac{1}{1 + [(k_s/k_w) - 1]0.75}\right\} \tag{2.12}$$

and,

$$F_a = \frac{1}{3}\left\{\frac{2}{1+[(k_a/k_w)-1]g_a} + \frac{1}{1+[(k_s/k_w)-1]g_c}\right\} \quad (2.13)$$

where g_a and g_c are the coefficients accounting for particle shape.

The values of g_i $(i = a, b, c)$ are difficult to be determined due to the randomness of soil particle shapes. Based on the assumptions, distinguishing whether water is considered as continuous pore fluid needs tremendous effort since in the field soil conditions are affected by many factors including soil gradation, soil mineralogy, etc. In addition, since Eq. (2.11) deals with moist unsaturated soils, in terms of dry soils, the De Vries method always provides lower thermal conductivity values.

2.4.1.3. Gori and Corasaniti model

Gori and Corasaniti (2002) proposed an enhanced unit cell model composed of a cubic space with a cubic solid particle at the center for predicting soil thermal conductivity. The soil moisture was categorized into four different ranges: $0 < \omega < W_c, W_c < \omega < W_p, W_p < \omega < W_f$, and $\omega > W_f$ (W_c, W_p, W_f are absorbed moisture content, wilting point, and field capacity of soils, respectively). The schematics of the model are illustrated in Figure 2-10.

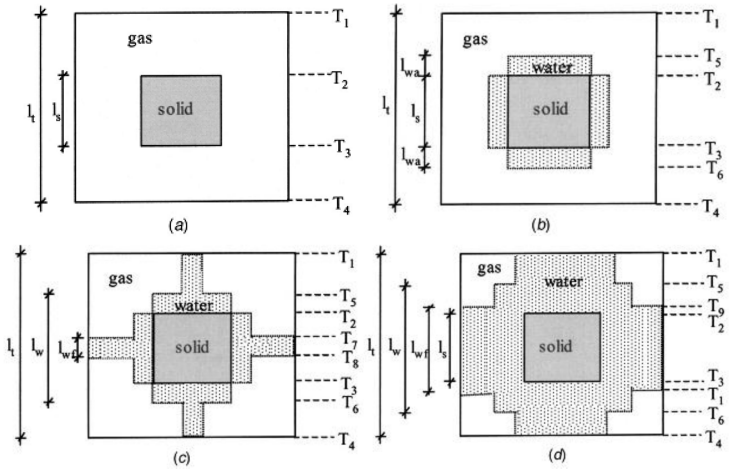

Figure 2- 10. Schematic illustrations of Gori and Corasaniti's model for unsaturated soils (Gori and Corasaniti, 2002).

The model predicts soil thermal behavior by solving the heat conduction equation with the assumption that parallel isotherms exit within the cubic space. The water bridge between soil particles forms at a moisture content equal to the wilting point. The effective thermal conductivities of soils are predicted separately in four regimes as aforementioned. This is not consistent with experimental results, where thermal conductivity is continuous with moisture content or degree of saturation. Another disadvantage of this model stem from the empirically determined dividing points for different types of soils.

2.4.1.4. Campbell model

The Campbell model (1994) is an extension of the De Vries model (1963). It is based on the assumption that the effective thermal conductivity of soil mixture (mineral, air, and water) can be expressed as the weighted sum of the thermal conductivities of the mixture components. The prediction of effective soil thermal conductivity can be expressed as

$$k_{eff} = \frac{F_s \phi_w k_w + F_s \phi_s k_s + F_a \phi_s k_a}{F_s \phi_w + F_s \phi_s + F_a \phi_s} \tag{2.14}$$

Compared to De Vries' method, this model only requires four parameters to specify thermal conductivity as a function of density, soil temperature, and water content. The parameters can be fitted to experimental data or predicted based on the physical properties of soils. The fitting parameters are comprised of the mineral fraction, the cutoff for water content recirculation, the power for the recirculation function, and a shape factor. Detailed information on model parameters is referred to Section 5.2. The Campbell model can accurately predict soil effective thermal conductivity for various soils and soil temperatures (Smits et al., 2013).

2.4.1.5. Tong model

Based on Wiener's theory (1912), Tong et al. (2009) proposed an effective thermal conductivity model, in closed form, for the simulation of thermo-hydro-mechanical processes of geological porous media. The model considers the effects

of mineral composition, temperature, degree of saturation, porosity, and pressure on the soil thermal conductivity. The developed model is constricted to Wiener bounds (isotropic and anisotropic mixtures) and Hashin-Shtrikman bounds (anisotropic mixture). The expression of the model is shown as

$$k_{eff} = \eta_1(1-\phi)k_s + (1-\eta_2)[1-\eta_1(1-\phi)]^2 \times \left[\frac{(1-\phi)(1-\eta_1)}{k_s} + \frac{\phi S_r}{k_w} + \frac{\phi(1-S_r)}{k_g}\right]^{-1} + \eta_2\left[(1-\phi)(1-\eta_1)k_s + \phi S_r k_w + \phi(1-S_r)k_g\right] \quad (2.15)$$

where k_g, k_s, and k_w are thermal conductivities of gas, solid, and water in a porous medium, respectively. ϕ is porosity. η_1 is the coefficient related to the pore structure of solid-water ϕ is the solid-gas mixture. η_2 is the coefficient as a function of porosity, saturation, and temperature.

Tong's model was verified only by bentonite, limiting its application. Although Tong et al. claimed that the model can be equally applied to assess the effective thermal conductivities of soils and rocks, the porosities corresponding to soils, bentonite, and rocks are different. General models need to be further developed.

2.4.1.6. Haigh model

Haigh et al. (2012) derived a unified model for evaluating soil thermal conductivity. The model simplifies the microstructure in the soils into three phases,

containing soil particles, pore water, and air. The expression of the model is shown as

$$\frac{k}{k_{solid}} = 2(1 + \xi)^2 \left\{ \frac{\alpha_w}{1-\alpha_w} \ln\left[\frac{(1+\xi)+(\alpha_w-1)x}{\xi+\alpha_w}\right] + \frac{\alpha_a}{(1-\alpha_a)^2} \ln\left[\frac{(1+\xi)}{(1+\xi)+(\alpha_a-1)x}\right] \right\} + \frac{2(1+\xi)}{(1-\alpha_w)(1-\alpha_a)} [(\alpha_w - \alpha_a)x - (1-\alpha_a)\alpha_w] \quad (2.16)$$

where α_w and α_a are the thermal conductivities of water and air normalized by the thermal conductivity of soil solids, respectively. ξ and x are parameters related to the degree of saturation and void ratio. The geometry of Haigh's mode is illustrated in Figure 2-11. β is the parameter related to saturation ratio.

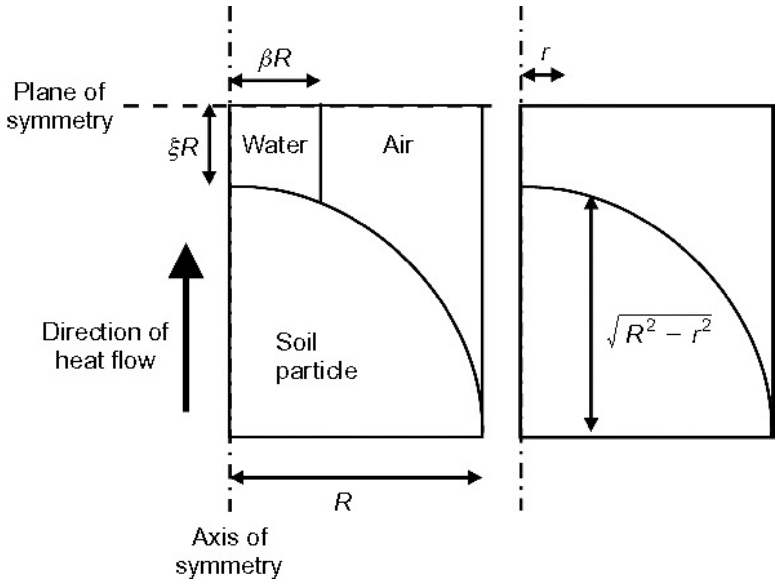

Figure 2- 11. Illustrations of the geometry of the axisymmetric contact model.

The Haigh model was validated by a variety of test measurements from the published literature for a wide range of sandy soils. This limits the model application to sands and the model might be inappropriate for other types of soils. In addition, the thermal conductivity of soils with porosity less than 0.33 cannot be evaluated by this model due to the limitation of the geometry of the soil unit cell itself.

2.4.2. Empirical models

2.4.2.1. Kersten model

Kersten (1949) measured the thermal properties of various types of clays, silts, and sands by using a line heat source in the laboratory, and proposed empirical equations for the evaluation of soil thermal conductivities by considering the effects of water content and dry bulk density. The equations are shown below.

For silt-clay,

$$k_{eff} = 0.1442 \times (0.9 \log \omega - 0.2) \cdot 10^{0.6243 \cdot \gamma_{dry}} \quad (2.17)$$

For sandy soils,

$$k_{eff} = 0.1442 \times (0.7 \log \omega + 0.4) \cdot 10^{0.6243 \cdot \gamma_{dry}} \quad (2.18)$$

where k_{eff} (W/(m·K)) is the effective thermal conductivity of soils; ω (%) is the moisture content; γ_{dry} (kg/m^3) is the dry bulk density.

Since all involved soil samples were tested under unsaturated conditions, the soil thermal conductivity at high degree of saturation can only be obtained by

extrapolating the experimental data. This empirical model might not be appropriate for soils at a high degree of saturation. Additionally, a discrepancy of approximately 25% or higher was found when the model was applied to high silt-clay content soils.

2.4.2.2. Johansen model

Johansen (1975) conceptualized a normalized thermal conductivity called Kersten number K_e. The Kersten number can be expressed by,

$$K_e = \frac{\left(k - k_{dry}\right)}{\left(k_{sat} - k_{dry}\right)} \tag{2.19}$$

where K_e is the Kersten number; k_{dry} and k_{sat} are the soil thermal conductivities at dry and saturated conditions, respectively.

A model was also proposed to describe the relationship between K_e and degree of saturation S by fitting the experimental data from Kersten's report (1949). First-order logarithmic functions were utilized to illustrate such relationships for different types of soils.

For medium and fine sands,

$$K_e = 0.7 \log(S) + 1 \tag{2.20}$$

For fine-grained soils,

$$K_e = \log(S) + 1 \tag{2.21}$$

For frozen medium, fine sands, and fine-grained soils,

$$K_e = S \tag{2.22}$$

The boundary at dry and saturate conditions was calculated to project Kersten numbers to the effective thermal conductivity. Thermal conductivities of single phase (solid, water, or gas) and other soil properties, including dry bulk density, porosity, and quartz content, were involved in the calculation. At dry conditions, a model was modified from De Vries' model (1963) to calculate k_{dry}.

$$k_{dry} = \frac{0.137\rho_d + 64.7}{2650 - 0.947\rho_d} \tag{2.23}$$

where ρ_d (kg/m3) is dry bulk density of soils.

In terms of k_{sat} involved in Eq. (2.20), this parameter can be calculated by Sass et al. (1971) equation,

$$k_{sat} = k_{water}^{n} k_{solid}^{1-n} \tag{2.24}$$

where k_{water} and k_{solid} (W/(m·K)) are thermal conductivity of water and solid, respectively.

Based on Eq. (2.19), Eq. (2.23), and Eq. (2.24), Johansen's soil thermal conductivity model can be expressed as follows,

$$k_{eff} = \left(k_{water}^{n} k_{solid}^{1-n} - \frac{0.137\rho_d + 64.7}{2650 - 0.947\rho_d}\right) K_e + \frac{0.137\rho_d + 64.7}{2650 - 0.947\rho_d} \tag{2.25}$$

Johansen's model was validated by the experimental data from Kersten's report and performed interpolation between the dry and saturated values of thermal conductivity of soils to evaluate the effective thermal conductivity. The thermal conductivities of silt and silty soils and sandy soils predicted by the model were 3

and 5 (W/(m·K)), respectively (Johansen, 1975). This indicated an overestimation of thermal conductivity of the model on clayey soils or clay and an underestimation on sandy soils containing relatively high quartz content.

2.4.2.3. Côté and Konrad model

Inspired by the Johansen model, Côté and Konrad derived a new empirical model based on the relative thermal conductivity. They established a hyperbolic equation for $K_e - S$ relationship by adding a fitted material parameter κ to Johansen's model. Further, a new equation was developed to determine dry thermal conductivity with two empirical parameters χ and η (Côté and Konrad, 2005a). The new $K_e - S$ relationship is given below.

$$K_e = \frac{\kappa S}{1 + (\kappa - 1)S} \tag{2.26}$$

where κ is the coefficient corresponding to the effects of soil types on $K_e - S$ relationship. The values of κ were suggested as 4.5, 3.55, and 1.9 for gravels; coarse sands, medium and fine sands, and silts; clayed soil and clay, respectively.

Furthermore, Côté and Konrad established a new equation for assessing the thermal conductivity of dry soils based on a large dataset from published literature. The relationship between the thermal conductivity of dry soils and porosity was examined. The influence of soil types on the thermal conductivity of dry soils is presented in Figure 2-12.

$$k_{dry} = \chi 10^{-\eta n} \tag{2.27}$$

where χ (W/(m·K)) and η are materials parameters related to the effect of particle shape; n is the porosity of soils. The recommended values of χ and η are 1.7 and 1.9 for crushed rocks, 0.75 and 1.2 for natural mineral soils, and 0.3 and 0.87 for organic fibrous soils or peat.

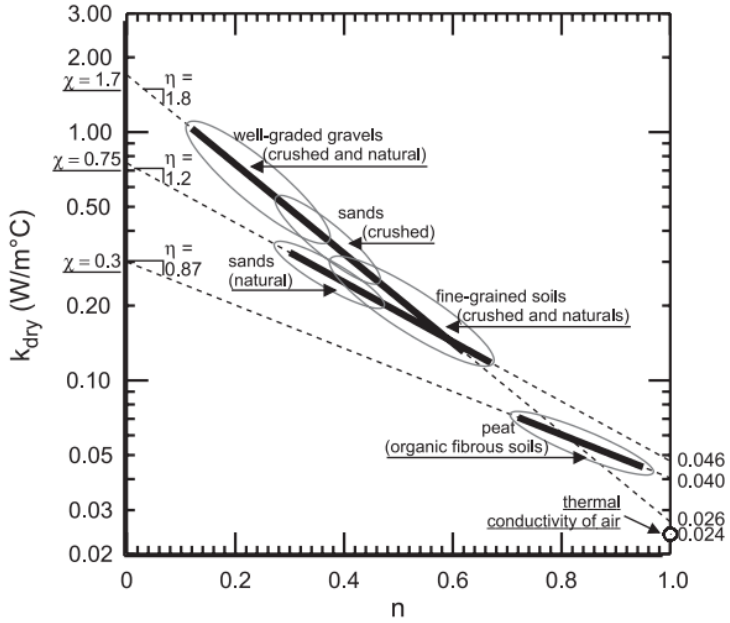

Figure 2- 12. Influence of soil type on k_dry (Côté and Konrad, 2005a).

In summary, the empirical model proposed by Côté and Konrad simultaneously examines the influences of soil type, soil degree of saturation, porosity, soil particle size and shape, and soil mineralogy on soil effective thermal conductivity. The mathematical expression of this mode is presented below.

$$k_{eff} = (k_{water}^{n} k_{solid}^{1-n} - \chi 10^{-\eta n}) \left[\frac{\kappa S}{1 + (\kappa - 1)S}\right] + \chi 10^{-\eta n} \quad (2.28)$$

The Côté and Konrad model can be applied to more soil types and exhibit a more accurate prediction of soil effective thermal conductivity than the Johansen model, reviewed in Section 2.4.2.2. Notwithstanding, improvements need to be conducted to provide continuous thermal conductivity prediction over the entire soil type range by investigating the limit value of κ between any two soil types.

2.4.2.4. Balland and Arp model

Previous empirical models considered the effects of soil minerals on effective thermal conductivity, but the influence of organic matter on soil thermal conductivity was not evaluated. Balland and Arp (2005) filled this research gap by modifying the thermal conductivity of the solid faction of soils in the Johansen (1975) method.

$$k_{solid} = k_{om}^{V_{om,s}} k_{quartz}^{V_{quartz,s}} k_{min}^{1-V_{om,s}-V_{quartz,s}} \quad (2.29)$$

where k_{om}, k_{quartz}, and k_{min} are thermal conductivities of organic matter, quartz, and other non-quartz minerals, respectively. $V_{om,s}$ and $V_{quartz,s}$ are the volume fraction of organic matter and quartz, respectively.

When soils are under dry conditions, the thermal conductivity can be calculated as,

$$k_{dry} = \frac{(ak_{solid} - k_{air})\rho_b + k_{air}\rho_p}{\rho_p - (1-a)\rho_b} \tag{2.30}$$

where $a = 0.053$. Note that this equation becomes Eq. (2.23) discussed in the Johansen method, when $k_{solid} = 3$ (W/(m·K)), $k_{air} = 0.024$ (W/(m·K)), and $\rho_p = 2.7$ (g/cm^3).

Therefore, the new $K_e - S$ relationship for unfrozen soils can be expressed by,

$$K_e = S^{0.5\left(1+V_{om,s}-\alpha V_{sand,s}-V_{cf,s}\right)}\left[\left(\frac{1}{1+exp(-\beta S)}\right)^3 - \left(\frac{1-S}{2}\right)^3\right]^{1-V_{om,s}} \tag{2.31}$$

where α and β denote adjustable parameters; $V_{sand,s}$ and $V_{cf,s}$ are the volumetric fractions of sand and coarse fragments within the soil solids, respectively.

The effective thermal conductivity of soils containing organic matter can be derived from Eq. (2.29), Eq. (2.30), and Eq. (2.31) according to the normalized thermal conductivity concept proposed by Johansen (1975). The model is suitable for soils at both low moisture levels and extremely high degrees of saturation. However, this model is limited to a temperature range from -30 to 30 ºC, which is not valid for wildfire effected soils under temperatures larger than 30 ºC.

2.4.2.5. Lu et al. model

An improved model, shown in Eq.(2.32), for estimating thermal conductivities of both coarse-textured and fine-textured soils from their volumetric water content was developed by Lu et al. (2007). The model is based on the normalized thermal conductivity concept with a new simplified linear $K_e - S$ relationship. Lu et al. stated that the relationship is dependent on the soil type, especially for fine grained soils.

$$k_{eff} = \left(k_{water}^{n} k_{solid}^{1-n} - (b - an)\right) \times exp[\alpha(1 - S^{\alpha - 1.33})] + (b - an) \quad (2.32)$$

where a and b are parameters related to the thermal conductivity of dry soils with values of 0.56 and 0.51, respectively. α denotes the effect of soil type on $K_e - S$ relationship. The suggested values of α for coarse soils and fine-grained soils are 0.96 and 0.27, respectively.

Lu et al.'s model is suitable for a bunch of soils, ranging from sand and sandy soils to clay and clayed soils. The prediction of thermal conductivity of soils agrees well with experimental data. Some limitations still exist that the quartz content of all tested soil samples was assumed as the same as sand samples, resulting in an overestimation of soil thermal conductivities. In addition, the thermal conductivity of dry soils predicted by this model may be not accurate due to no consideration of the effect of soil type.

2.4.2.6. Chen model

Chen (2008) developed a model with high accuracy for the prediction of thermal conductivity of sands with high quartz content, which filled the research gap from previous studies. The relationship between thermal conductivity and porosity/degree of saturation was examined in this model. And a power exponential function was selected to establish the model for sands.

$$k_{eff} = k_{water}^{n} k_{solid}^{1-n} [(1-b)S + b]^{cn} \quad (2.33)$$

where b and c are empirical parameters with suggested values of 0.0022 and 0.78, respectively.

Chen's model greatly improved the prediction accuracy of thermal conductivities for quartz sands. And the model needs fewer model parameters compared to Johansen's (1975) model. From other inspections, these advantages act also as disadvantages of the model in that the model is limited to sands.

2.4.2.7. Zhang et al. model

Zhang et al. (2017a) proposed a new empirical thermal conductivity prediction model accounting for the effects of moisture content, dry density, quartz content, and soil type on soil thermal conductivity. The model was validated by data from existing literature and laboratory test results obtained by thermo-time domain reflectometry (TDR) techniques. In this model, the $K_e - S$ relationship was

modified to evaluate the effect of quartz content on thermal conductivity, as shown below.

$$k_e = \frac{[2.168 \times 10^{-5} \times exp(x/7.903) + 1.252]S}{1 + [2.168 \times 10^{-5} \times exp(x/7.903) + 1.252]S} \tag{2.34}$$

where x (%) is the quartz content.

The continuum thermal conductivity model is expressed in the following based on the normalized thermal conductivity concept.

$$k_{eff} = \frac{[2.168\times10^{-5}\times exp(x/7.903)+1.252]S}{1+[2.168\times10^{-5}\times exp(x/7.903)+1.252]S} \times \tag{2.35}$$

$$\left[k_{water}^{n}\left(k_{quartz}^{x/100}k_{kaolin}^{1-x/100}\right)^{1-n} - (1.216 \times 10^{-5} \times exp(x/6.599) + 3.034) \times 10^{[-0.003\times exp(x/16.542)-1.84]\times n}\right] + (1.216 \times 10^{-5} \times exp(x/6.599) + 3.034) \times 10^{[-0.003\times exp(x/16.542)-1.84]\times n}$$

where k_{water}, k_{quartz}, and k_{kaolin} are thermal conductivity of water, quartz, and kaolinite, respectively.

This new generalized model was found to be in relatively good agreement with experimental data, indicating a potential application in the field of energy geotechnics. However, the shortcoming of this model is that it only considers the effects of environmental factors and compositional factors, and no chemical factors (i.e., organic matter, contamination) are examined.

2.4.3. Other models

2.4.3.1. Donazzi Model

The thermal behavior of the soil surrounding buried cables was investigated by Donazzi et al. (1979) using thermo-time domain reflectometry. Based on the experimental results, a model related to soil thermal resistivity was proposed and validated. The model expression is as follows,

$$\rho = \rho_w^n \rho_o^{1-n} exp[3.08(1-S)n] \quad (2.36)$$

where ρ_w is the thermal resistivity of water with a value of 1.70 ((m·K/W); ρ_o is the thermal resistivity of bulk material.

The model was initially developed to evaluate the thermal behavior of backfill soils around buried cables during the cable service period. Two typical parameters, namely degree of saturation and porosity, were involved in the investigation. While this model did not consider the effect of organic matter, probably produced by surface vegetations during cables' long service term, on the soil thermal conductivity.

2.4.3.2. Gangadhara Rao and Singh model

To predict the thermal resistivity of soils more accurately, Gangadhara Rao and Singh (1999) established an empirical relationship to estimate the thermal resistivity of four types of soils. The model deals with the dependence of thermal

resistivity on soil moisture content and density. The thermal resistivity can be calculated as,

$$\rho = [1.07 \log \omega + b]^{-1} \times 10^{(3-0.01\gamma)} \quad (2.37)$$

where ω is soil water content; γ (lb/ft^3) is the dry unit weight of soil, and b is the empirical parameter dependent on the type of soil.

The model stemmed from curve fittings to the measured thermal resistivity in the laboratory under various moisture contents and dry densities scenarios. The predicted resistivity has an absolute difference of 10-15% from the laboratory test results.

2.4.3.3. Zhang et al. model

To eliminate irrational correlations between soil thermal conductivity and its influencing factors stemming from sample insufficiency, Zhang et al. (2020) proposed a unified thermal conductivity model based on a screened artificial neural network approach. The algorithm of the approach is illustrated in Figure 2-13.

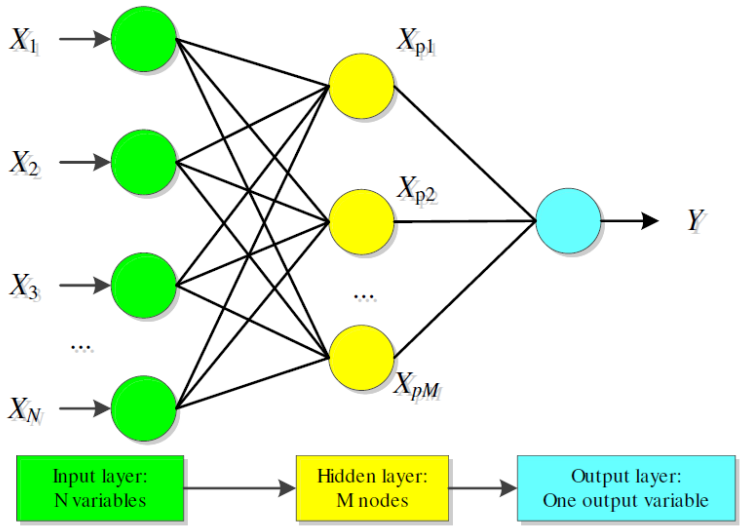

Figure 2- 13. The Algorithm of back-propagation artificial neural network (Zhang et al., 2020).

Several factors, including dry density, porosity, degree of saturation, quartz content, sand content, and clay content, were considered by the artificial neural network to estimate the parameter κ, a key coefficient for the normalized thermal conductivity concept. Based on the predicted κ, the soil thermal conductivity was estimated via Côté and Konrad's (2005a) model. Zhang et al. utilized 257 soil thermal conductivity measurements collected from the literature as a database to perform the evaluation. The obtained κ ranges from 1.31 to 7.61 and predicted thermal conductivities agree well with measured data. Although Zhang et al. provided easy-to-use contours to estimate κ, the measured thermal conductivities, which form the database, have not considered chemical effects. This model may

provide less accurate results when predicting thermal conductivities of soils with chemical effects, such as contamination and wildfire-induced organic matter.

2.5. Summary and Major Research Gaps

This chapter introduces the fundamentals of water repellent soils, the effects of hydrophobicity on soil thermal and hydraulic properties, and existing soil thermal conductivity prediction models. Following the literature review, the knowledge gaps are specified as below.

1. Isolated impacts of water repellency on backfill materials in the energy application field are in need. Literature documented in Section 2.2 summarizes the fundamentals of hydrophobicity and origins of soil water repellency including wildfires and fungi. Chapter 3 proposes to use dimethyldichlorosilane to induce soil hydrophobicity to simulate naturally occurring water repellency on soils. Surface characterizations are conducted to verify the hydrophobicity. Artificially induced water repellent sands are used to investigate the isolated impacts on soil thermal and hydraulic properties.

2. The thermal behavior of water repellent soils is insufficiently investigated. Section 2.3.1 shows that several contradictions

occurred in previous studies, the thermal properties of water repellent soils, especially thermal conductivity, need a deeper and more sophisticated investigation considering the effect of water content or degree of saturation. The thermal conductivity of hydrophobic sands with respect to the degree of saturation is carried out by laboratory tests in Chapter 4. The thermal response of regular sands (hydrophilic) is also investigated as a comparison. In addition, impacts of the degree of water repellency on soil thermal conductivity are evaluated.

3. Prediction models for thermal conductivity of hydrophobic soils have not yet been studied. Although the thermal conductivity models have been widely used in soil science and geotechnical engineering, as summarized in Section 2.4, the existing models have accounted for the effects of environmental and compositional factors but no chemical factors (viz. surface wettability). Chapter 5 presents the development of a new thermal conductivity prediction model, modified from Campbell's (1994) model, for hydrophobic sands. The model is validated by experimental data and accounts for the thermal conductivity response for the entire saturation range.

CHAPTER 3. SOIL HYDROPHOBIZATION AND SURFACE CHARACTERIZATION

3.1. Introduction

In the laboratory, controlled water repellency of soils can be achieved by coating the soil particles with organic substances (Morley et al., 2005b), silanes (Bachmann et al., 2003), polymers (Dong, 2013), and carbon nanotubes (Dorrer and Rühe, 2008). In nature, organic compounds stemming from vegetation or wildfires induce soil water repellency. Doerr et al. (2005) and Morley et al. (2005a) extracted organic compounds from water-repellent sandy soils and further identified typical groups of compounds by utilizing gas chromatography-mass spectrometry (GC-MS). They found that long-chain acids, alkanes, amides, aldehydes/ketones, and sterols were the main groups of compounds inducing soil hydrophobicity. The effects of those compounds on water repellency of soils have been performed using stearic acid (Leelamanie et al., 2008; Lourenço et al., 2015) and oleic acid (Wijewardana, Senani, N. et al., 2015). However, no in-depth studies on the impacts of individual organic compounds were conducted until the publishing of Mainwaring et al.'s work (Mainwaring et al., 2013). Depending on

the identified organic compounds by GC-MS, their study detailed investigated the effects of chain length, molecular shape, functional group, heating, particle size, and packing efficiency on soil wettability. And the results revealed that individual compounds cannot induce repellency on acid-washed sand at loadings equivalent to the level of detection of individual compounds in hydrophobic soils by GC-MS. A combination of long-chain acid and alkene will be effective at inducing water repellency (Lourenço et al., 2015; Mainwaring et al., 2013). However, from a sample preparation perspective, except for dissolved organic carbon, other types of organic compounds such as stearic acid and oleic acid needs a solvent to help to mix with soils due to their low solubility in water, making the preparation complicated and costly.

Compared with organic compounds, individual use of silane can induce higher and more stable water repellency, and share common chemistry (Figure 1-5), making them more suitable for soil surface treatment (Bachmann et al., 2003; Chan and Lourenço, 2016). The process of sanitation on soils is that silanes react with residual water soil particle surface and silica surface to form new hydrophobic polymers as shown in Figure 1-5. Three types of silanes, namely, dimethyldichlorosilane $(CH_3)_2SiCl_2$ (DMDCS), octadecyltrichlorosilane $CH_3(CH_2)_{17}SiCl_3$ (OTS), and trimethylchlorosilane $(CH_3)_3SiCl$ (TMCS), share a similar reaction mechanism with silica (Chan and Lourenço, 2016). Both DCDMS (Bachmann et al., 2003; Chan and Lourenço, 2016), OTS (Ahmed and van Geel,

2009), and TMCS (Chan and Lourenço, 2016) can be directly mixed with soils and have been applied to induce soil water repellency. Chan et al. (2016) systematically examined the water repellent characteristics of the three silanes including maximum water repellency, time stability, and conditions to enhance their hydrophobicity. The silanes were proved to induce high and stable water repellency. Another type of coating on soils was also studied, namely, polymer coating. Dong (2013) coated a thermally sensitive polymer to soils using the surface-initiated atom transfer radical polymerization technique. The obtained treated sand particles behave as designed that at room temperature, coated sands are hydrophilic; while heated to 50 ºC, they turn to be hydrophobic. This 'smart soil' has potential applications for intelligent hydraulic barriers and oil-water separation due to its susceptible properties to temperature variations. However, unlike silane treatments with a simple coating process, this polymer coating process is complicated with four steps: surface cleaning and hydroxylation, amino-ended silanization, initiator anchoring, and polymerization of NIPAAm on the initiator-modified surface to form polymer chains (Dong, 2013). Therefore, silane coating may be more cost-benefit if the hydrophobicity of soils is the only requirement, and no environmental adjustment of treated soils is needed.

3.2. Materials

Two uniform granular materials with different grain sizes were selected in this study for producing hydrophobic sands using silanization. The sands were Ottawa 20/30 sand (D_{50} = 0.72 mm) and Ottawa 50/70 sand (D_{50} = 0.35 mm), as presented in Figure 3-1. Manufactured by US Silica, the sands are clean, siliceous sand with a considerably rounded shape and classified as poorly graded sand as shown in Figure 3-2. Both Ottawa 20/30 and 50/70 sand consist of 99.8% quartz, based on the X-ray diffraction analysis. Other physical properties of the sands are summarized in Table 3-1. The chemical, dichlorodimethylsilane (DMDCS, 99.5%), was purchased from Sigma Aldrich (St. Louis) and used as received.

(a) (b)

Figure 3- 1. The Ottawa sands used in this study: (a) 20/30 sand; (b) 50/70 sand.

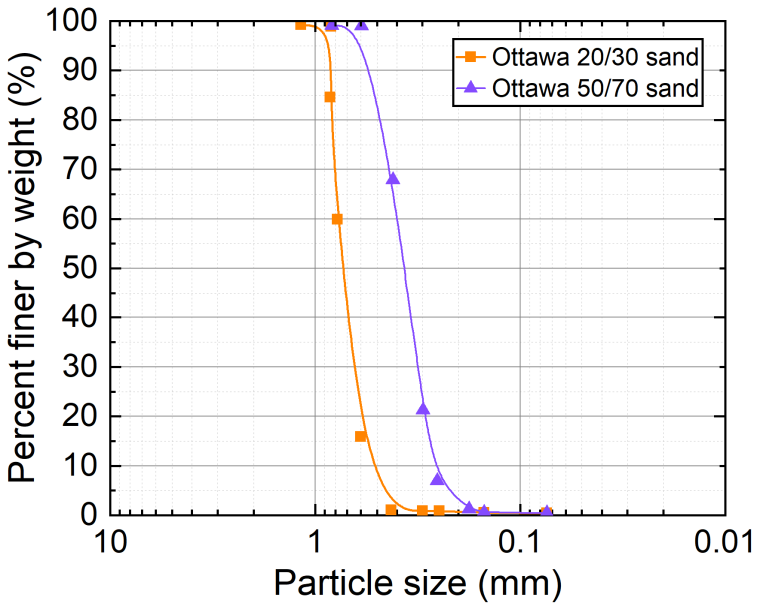

Figure 3- 2. Particle size distributions of Ottawa 20/30 sand and Ottawa 50/70 sand.

Table 3-1. Physical properties of Ottawa 20/30 and 50/70 sand.

Properties	**Ottawa 20/30 sand**	**Ottawa 50/70 sand**
Mineralogy	quartz	quartz
Specific gravity, G_s	2.65	2.65
D_{50} (mm)	0.72	0.35
Maximum void ratio, e_{max}	0.74	0.85
Minimum void ratio, e_{min}	0.50	0.59
Coefficient of uniformity, C_u	1.15	1.43

3.3. Soil Hydrophobization

3.3.1. Soil treatment

In this study, the Ottawa sands were hydrophobized by gradually applying DMDCS to air-dried sand samples with a pipette. The level of induced water repellency depends on DMDCS concentration and soil type (Bachmann et al., 2001; Ng and Lourenço, 2016). According to Zheng's investigations on the influence of the DMDCS concentration on the contact angle of standard Fujian sand (Zheng, 2019), the solution rate of DMDCS, 20 $mL \cdot kg^{-1}$ for Ottawa 20/30 sand and 40 $mL \cdot kg^{-1}$ for Ottawa 50/70 sand, was determined to produce extreme water repellency. The target sand samples were washed using de-ionized (DI) water and air-dried before treatment. When performing treatments, a targeted amount of DMDCS was added to air-dried sand samples using a micropipette, mixed and stirred with a rod for 2 minutes. The whole process occurred within a fume hood to avoid the inhalation of hydrogen chloride (HCl) gas generated during the chemical reaction. During the hydrophobization process, DMDCS reacted with residual water molecules settled on sand particle surfaces. This reaction produced a water repellent coating, polydimethylsiloxane (PDMS), and HCl gas as a by-product, as shown in Eq. (3-1). A thin layer of PDMS was bonded to sand particle surfaces,

isolating particles from water. The treated samples were put in the fume hood for 3 days to reach a relatively stable contact angle (Zheng, 2019). After 3 days, the coated samples were rinsed with DI water to remove possible hydrogen acid residue and then air-dried.

$$n[(CH_3)_2SiCl_2] + n[H_2O] \rightarrow [(CH_3)_2SiO]_n + 2nHCl \quad (3\text{-}1)$$

where n is the number of repeating monomer unit. The interaction between the oxygen atoms of PDMS molecules and the polar groups (such as -OH groups) on sand particle surfaces resulted in outward orientations of the methyl (-CH3) groups of PDMS molecules from sand particle surfaces. This phenomenon, as illustrated in Figure 3-3, produced highly hydrophobicity of particles (Goebel et al., 2007). In addition, the specific gravity (G_s) of treated sand was carried out following the standard ASTM D854-14 (2014). The G_s of treated Ottawa 20/30 sand and treated Ottawa 50/70 sand is 2.62 and 2.49, respectively, lower than that of untreated sands (Table 3-1). The formation of the PDMS coatings on sand particles contributed to the lower G_s since the coating has a smaller specific gravity (1.04-1.51) than sand (Owen, 2001). The influence of PDMS on G_s was discussed in detail by Liu et al. (2020).

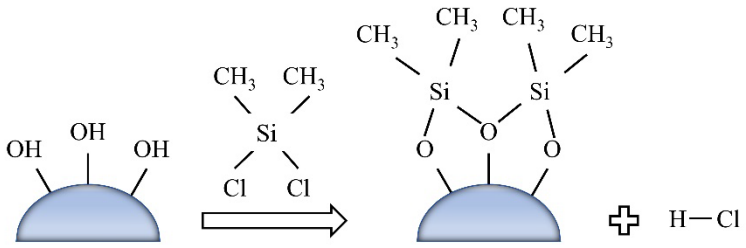

Figure 3- 3. Schematic view of silane formation (monolayer) on the surface of silica surface for DMDCS.

3.3.2. Hydrophobicity measurement

The assessment of soil hydrophobicity has been summarized in Section 2.2.3. Among the discussed techniques, two measuring methods were adopted in this study to evaluate the degree of water repellency of different sand samples: the sessile drop method (SDM) and water drop penetration time (WDPT).

3.3.2.1. Sessile drop method (SDM)

The apparent contact angle was conducted using the sessile drop method with a Ramé-hart Model 250 goniometer (Figure 3-4). According to Bachmann's method (2000), a smoothie microscope glass slide was covered with a double-sided adhesive tape (EZlifego, USA). Sand samples were air dried and subsequently spayed on the tape. Sand particles were carefully pressed to the tape using a spare glass slide for 3 to 5 s. Then the slide was shaken conscientiously to remove surplus grains to obtain a relative monolayer of sand, as shown in Figure 3-5. Contact angles were measured after sample preparation using a goniometer. The room

temperature and relative humidity during the measurement were around 22 ºC and around 80%, respectively. Three drops of deionized water (drop volume was 10 µL) were placed on the specimen surface using a syringe. The shape of the water drop was immediately recorded by a camera within 1 min. Then the contact angle determined based on the curve-fitting technique proposed by Saulick et al. (2017). For each specimen, the apparent contact angle was determined by averaging the three measured angles.

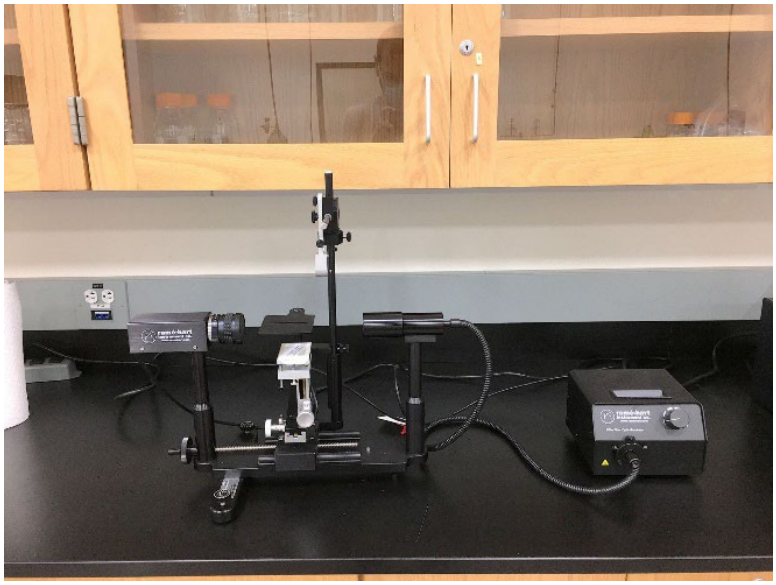

Figure 3- 4. Goniometer used for sessile drop method (Ramé-hart Model 250).

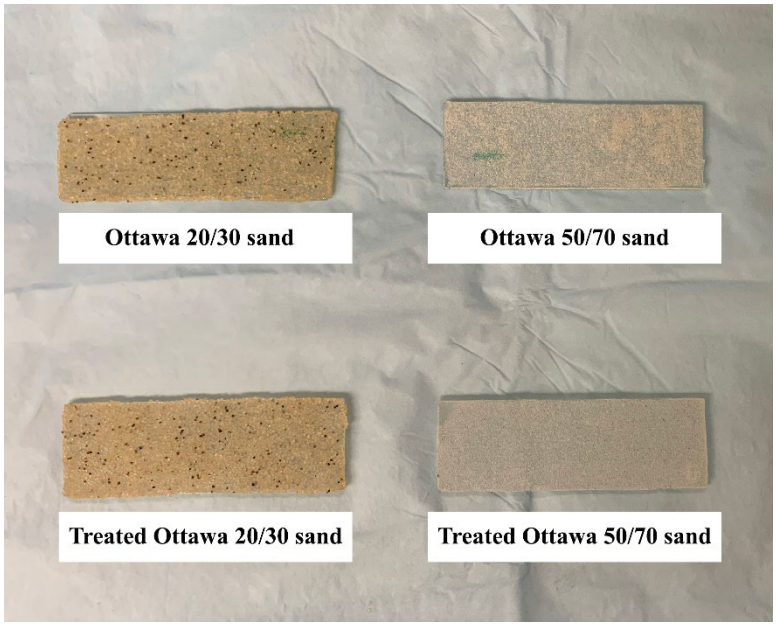

Figure 3- 5. Specimens for contact angle measurements.

The apparent contact angle of regular Ottawa 20/30 and 50/70 sand are around 43.6º and 33.7º, respectively, meaning that the two sands are hydrophilic as shown in Figure 3-6. The apparent contact angles of treated Ottawa 20/30 and 50/70 are 116.6º and 142.4º, respectively. The results illustrated that the DMDCS induced an extremely hydrophobicity on sand samples with a contact angle larger than 90º.

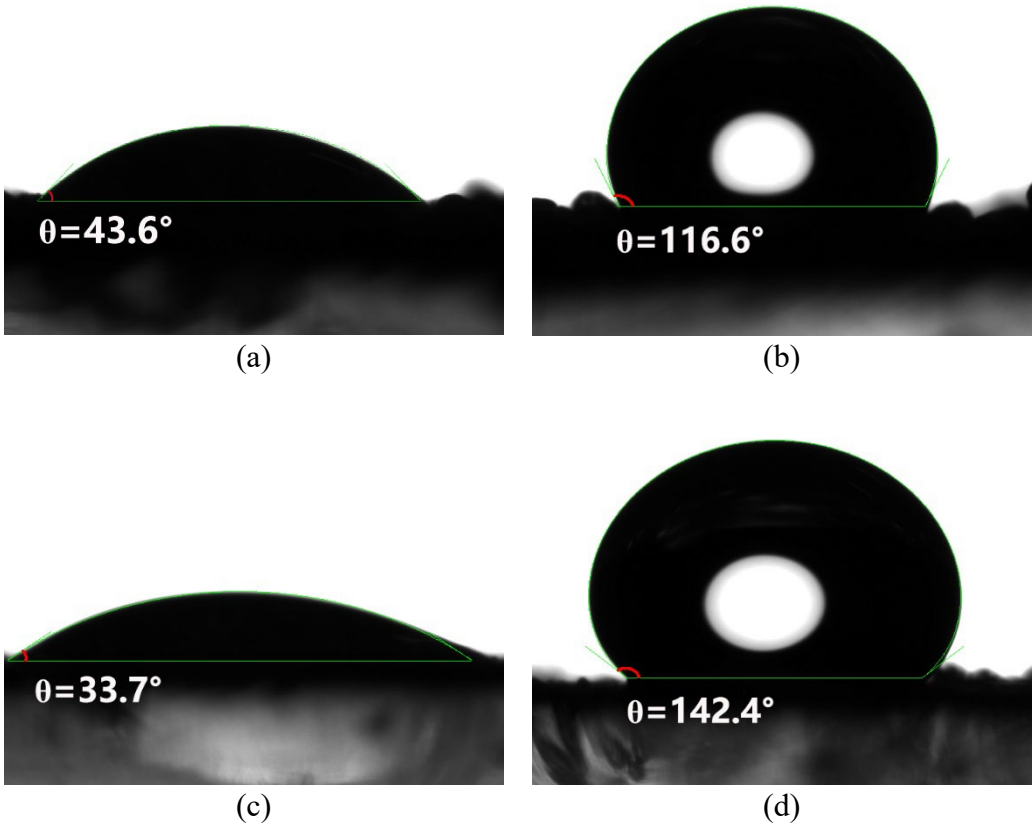

Figure 3- 6. Contact angle measurement for (a) Ottawa 20/30 sand, (b) treated Ottawa 20/30 sand, (c) Ottawa 50/70 sand, and (d) treated Ottawa 50/70 sand.

3.3.2.2. Water drop penetration time (WDPT) test

Sand water repellency was also estimated using the water drop penetration time (WDPT) method (Doerr et al., 2000), which is simple and practical (Letey et al., 2000). This method measures the time needed by the distilled water droplet (on the sample surface) to penetrate into the sand sample. The volume of water droplets involved in WDPT test varies between 50 and 80 µL (Lourenço et al., 2015). In this

study, sand samples were firstly air-dried and pluviated into a petri dish with an inner diameter and height of 6.6 cm and 1.5 cm, respectively. The surface of the sample was then made flat. Water drops with a volume of 50 μL, greater than the particle size and voids (Letey et al., 2000), were placed on the flat sample surface. The samples were covered to minimize evaporation. The measurements were conducted in a laboratory environment with a room temperature of 23 ºC and humidity ranging from 60% to 70%. The time for WDPT test was up to 14400s (Shakesby and Doerr, 2006).

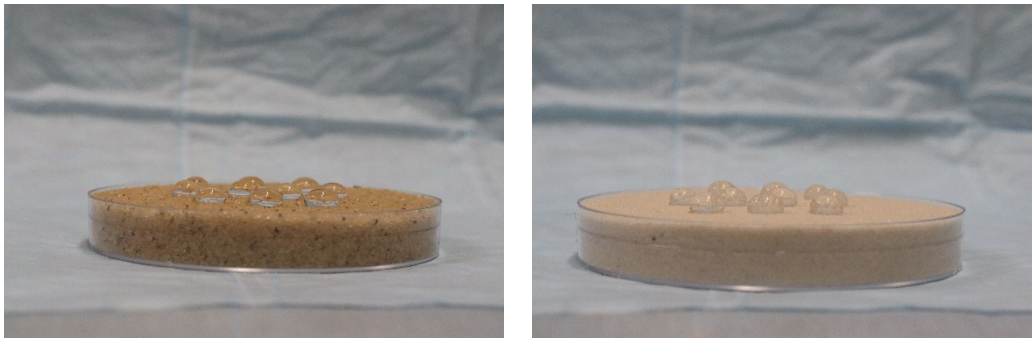

(a) (b)

Figure 3- 7. WDPT test for hydrophobic sands: (a) Ottawa 20/30 sand and (b) Ottawa 50/70 sand.

Table 3- 1. Water repellency classification using the WDPT method for the regular and artificially hydrophobized sands.

Soil texture	WDPT (s)	Classification
Ottawa 20/30 sand	<5	Wettable
Treated 20/30 sand	>3600	Extremely water repellent
Ottawa 50/70 sand	<5	Wettable
Treated Ottawa 50/70 sand	>3600	Extremely water repellent

3.4. Surface Characterization

Characterizations of the modified sand particle surface were performed using SEM (scanning electron microscopy), EDS (energy dispersive spectroscopy), and Raman Microscopy.

3.4.1. Instrumentation

A Hitachi S-4800 II field-emission SEM (FE-SEM) system with an ultra-high-resolution of 1.0 nm/30 kV, which is also capable of ultra-low voltage imaging (0.5 kV), was utilized to collect SEM images on sand particles. A Hitachi S-3000N system with variable pressure SEM and equipped with an UltraDry EDS detector and electron backscatter diffraction (EBSD) camera contributed to the evaluation of elemental compositions of treated and untreated sands. The acceleration voltage and working distance involved in the EDS analysis were 15 kV and 14 mm, respectively. Raman spectrum of sand samples was carried out using a DXR3 Raman spectrometer (Thermo Fisher Scientific) equipped with a green laser (wavelength λ=532 nm), an electro-multiplier CCD detector, and an Olympus BX41 microscope. The Raman backscattering was recorded at an exposure time of 30 s for 5 accumulation scans for all samples, which benefits in reducing the fluorescence background. More than two Raman measurements were taken utilizing the 100× objective for each sample.

3.4.2. SEM characterization

The surface morphology of DMDCS treated and untreated sand particles at different magnifications were presented by scanning electron microscopic images (Figure 3-8). The particle size of sand samples was approximately 75 mm. Small cracks and bumps were observed on the sand particle surface in the 100× image (Figure 3-8(a)), which significantly increased surface roughness. Fragments and chips were detected to be attached to the grain surface with 1k× magnification (Figure 3-8(c)). The shape and size of the chips and fragments were illustrated in Figure 3-8(d). The SEM microphotographs of the untreated sand particle are shown in Figures 3-8(e) – (h). Similar fragments were also discovered on untreated sand surfaces. Conclusions cannot be drawn that those chips and fragments are the PDMS coatings, by simply comparing both treated and untreated sand particle SEM images. One other reason is that coating may not be visible for the DMDCS-treated sand due to the thickness of the PDMS layer being in the order of nm to μm (Lin, 2020). Notwithstanding, arrays of chips and fragments on micrometer and nanometer scales greatly increased the roughness of the grain surface, enhancing the surface hydrophobicity.

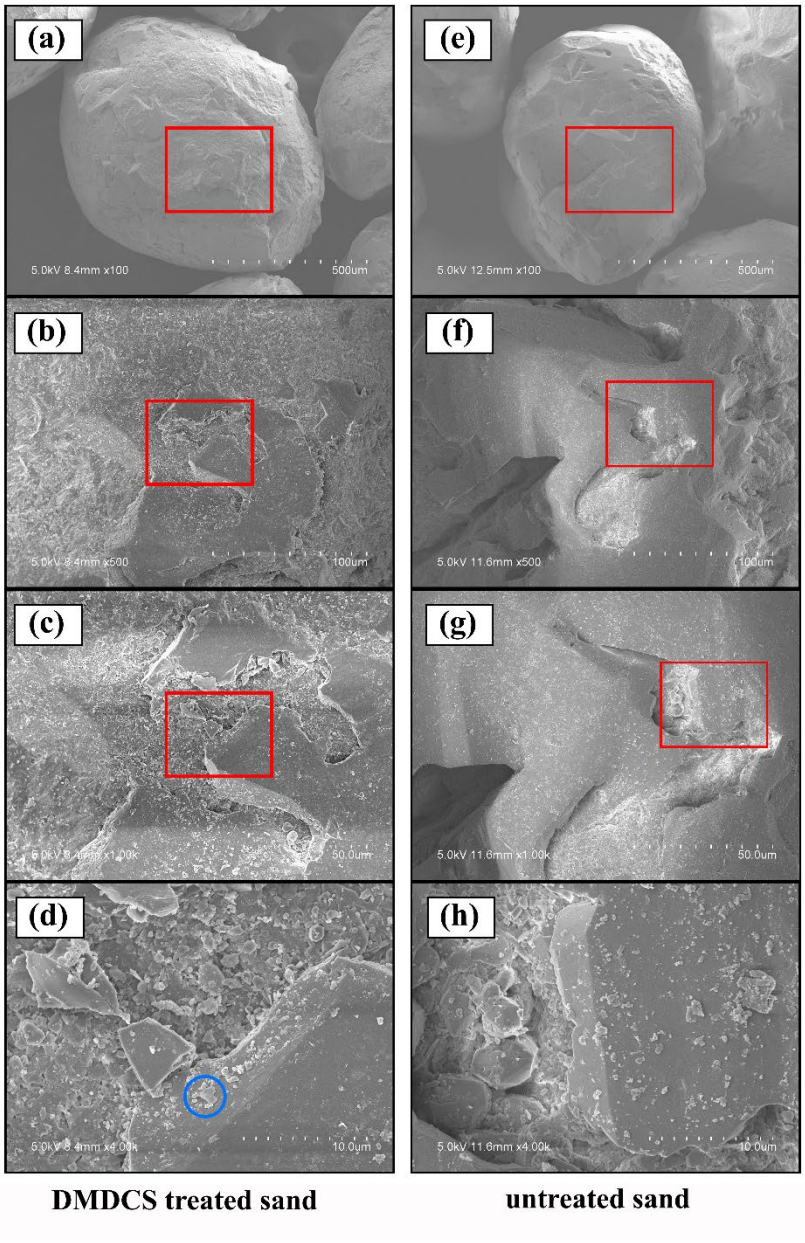

Figure 3- 8. SEM images in terms of DMDCS treated sand (Ottawa 20/30) at different magnifications: (a) whole sand particle, (b) zoomed on a surface crack, (c) and (d) fragments enhancing surface roughness, and (e)-(f) untreated sand.

3.4.3. SEM-EDS characterization of surface chemical composition

The determination of the elemental composition of treated and untreated sands was conducted by the SEM-EDS technique. In the analysis, backscattered images were obtained by SEM, and the chemical compositions were analyzed with EDS. The point analysis was used to determine the element composition of different locations of sand particle surfaces, as shown in Figure 3-9(a) and (c) for untreated and treated Ottawa 20/30 sand. Example spectrums are presented in Figure 3-9(b) and (d). Table 3-2 summarizes the corresponding results of point analyses. The H element contained in the sample is not detected due to its small density. From the EDS analysis, enrichment of the C element occurred possibly due to the hydrophobization. The water repellent coating, polydimethylsiloxane (PDMS, $[(CH_3)_2SiO]_n$), formed on the sand surface, has dramatically increased the atomic percent of the C element. Compared to untreated sand, the atomic percent of C element on the treated sand surface increased by 277.6%. To verify the formation of PDMS, Raman spectral measurements were performed on both untreated and treated sand particle surfaces, which are detailed in the following section.

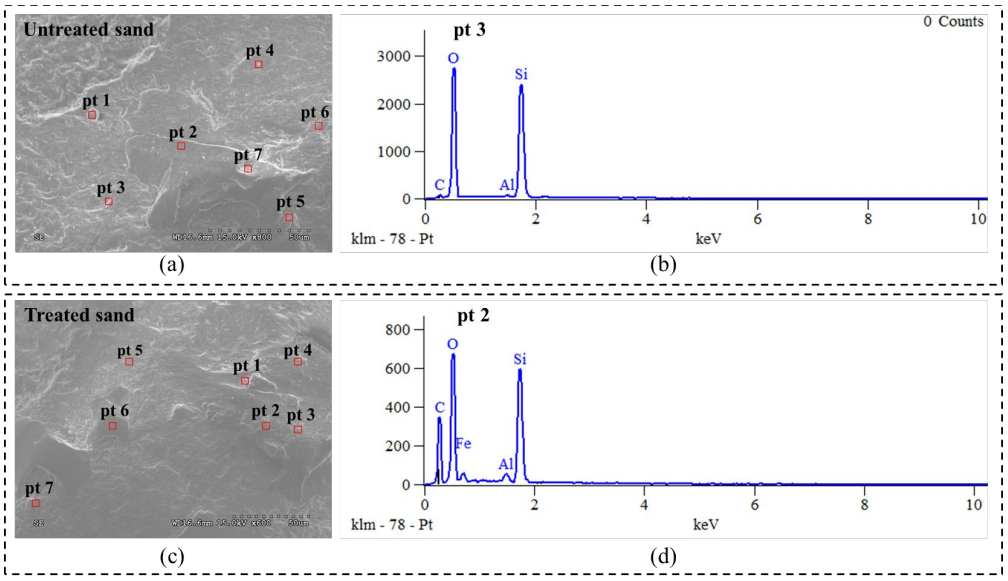

Figure 3- 9. SEM morphologies and example EDS spectrum of (a) and (b) untreated Ottawa 20/30 sand and (c) and (d) treated Ottawa 20/30 sand, respectively.

3.4.4. Raman characterization of surface modification

Raman spectroscopy was utilized to characterize the molecular structure of both untreated and treated Ottawa 20/30 sand samples. In order to facilitate the Raman measurements, doubled-sided tapes were attached to a sample holder. Then, several randomly picked sand particles were sprayed on the tape. The Raman spectra of untreated and treated sand samples, using the Raman microscope at λ=532 nm, were acquired (Figure 3-10). These spectra present characteristic Raman vibrational modes. Compared to untreated sand spectra, the treated one has two strong peaks at 2904 and 2965 cm^{-1}. The two peaks correspond to the symmetric

and antisymmetric -CH3 stretching vibrations (Socrates, 2015), indicating that the hydrophobic PDMS has been formed and adhered to the treated sand surface.

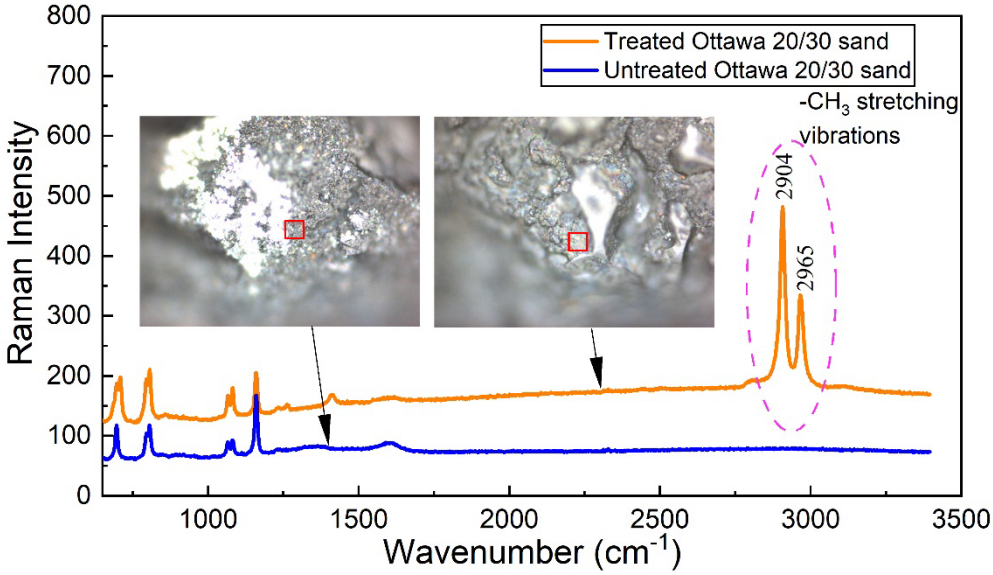

Figure 3- 10. Raman spectrum of untreated and treated Ottawa 20/30 sand.

3.5. Summary

In this chapter, all two Ottawa sands (20/30 and 50/70) involved in this dissertation study and the soil treatment method were introduced. Several surface characterization methods were utilized to verify the product (PDMS), stemming from the chemical reaction, on sand surfaces. The SEM-EDS results presented the enrichment of the atomic percent of C element on the treated sand surface possibly due to the formation of PDMS. In addition, the Raman spectra indicted that a thin layer of PDMS (hydrophobic) successfully formed on the sand.

Table 3- 2. The element composition of the marked spots in Figure 3-9 on untreated and treated sand surfaces.

Element	Pt 1		Pt 2		Pt 3		Pt 4		Pt 5		Pt 6		Pt 7	
	U.T.	Tr.	U.T.	Tr.	U.T.	Tr.	U.T.	Tr.	U.T.	Tr.	U.T.	Tr.	U.T.	Tr.
C (%)	12.87	50.36	8.18	50.73	9.43	51.58	9.92	41.47	8.78	21.67	8.71	18.91	9.90	20.1
O (%)	59.28	36.71	70.15	40.32	68.54	36.94	68.55	46.54	67.48	64.88	63.33	66.77	66.18	59.63
F (%)						1.16		0.48			5.74			6.92
Al (%)	0.62		0.10	0.65	0.31	0.44		0.77			0.71			
Si (%)	25.59	12.92	21.56	8.14	21.72	9.88	21.53	10.74	23.47	13.46	20.66	14.32	23.92	13.44
S (%)	0.15										0.80			
Ca (%)											0.95			
Fe (%)	1.50			0.17										
Br (%)									0.26					

*U.T. and Tr. denote untreated sand and treated sand, respectively.

CHAPTER 4. THERMAL PROPERTIES OF SANDS WITH VARIOUS WATER REPELLENCY

4.1. Introduction

The heat transfer process in soils depends on soil thermal conductivity and is affected by many factors including soil gradation, mineralogy components, soil wettability et al. Soil thermal conductivity has been involved in many geothermal applications, such as geothermal energy piles and borehole thermal energy storage, etc. Some of the energy systems are generally shallowly buried, where part of soils interacted with the system may be water repellent due to influences of contaminations and plant roots.

This chapter presents laboratory studies on quartz sands with various water repellencies using the KD2 standard probe. The effects of moisture content, dry density, and level of water repellency on soil thermal conductivity were examined.

4.2. Materials

Thermal conductivity evaluations of hydrophilic and hydrophobic sands were performed by using KD2 thermal probe. The test parameters considered in this study are moisture content, dry density, and level of water repellency. The selected sands were Ottawa 20/30 sand, Ottawa 50/70 sand, and their hydrophobic counterparts. In addition, mixtures of hydrophobic and hydrophilic sands were used to simulate different degrees of water repellency. The untreated sand samples were mixed with the treated counterparts (extremely water-repellent) at different mass ratios, namely, 10:0, 9:1, 8:2, and 0:10, to provide sand samples with various degrees of water repellency. The mass ratio means the ratio of wettable sand to extremely water-repellent sand; for instance, the ratio of 9:1 means 9 grams of wettable sand mixed with 1 gram of its hydrophobic counterpart. The degree of sample water repellency is determined by WDPT test. Table 4-1 summarized the classification of water repellency of the hydrophobized sand samples based on the WDPT method. The wettable (untreated) sands (no hydrophobic samples added) had a WDPT of less than 5 sec, while the completely water repellent sand samples (100% hydrophobic sands) displayed a WDPT larger than 3600 sec. Sand wettability is susceptible to a small amount of water repellent particles, especially for fine-grained sand (Ottawa 50/70 sand), which was indicated by the increase of

WDPT with the ratio of wettable sample to extremely hydrophobic sample. The physical properties of hydrophilic 20/30 and 50/70 sands were presented in Table 3-1. The technique for producing hydrophobic sand was discussed in section 3.3.1. The target moisture content and actual dry density range of sand samples were illustrated in Table 4-1.

4.3. Experimental Setup and Program

4.3.1. Experimental setup and test program

Soil specimens were prepared by applying the following procedures. The dry sand was first thoroughly mixed with deionized water to reach various target moisture contents. Three moist sand samples were then compacted using a rammer with 5 drops per soil layer in PVC plastic modes with an average inner height of 76 mm and a diameter of 78 mm. Samples were compacted in three layers to achieve the desired height. After compaction, the specimens were wrapped with plastics, horizontally laid to reduce the effect of gravity during moisture redistribution, and left for 24 hours at room temperature to obtain uniformly distributed moisture. The targe moisture contents of three tested sands are given in Table 4-1.

Table 4- 1. Target moisture contents of test materials.

Sand	Mixture Code	Ratio†	Target moisture content (%)	Actual dry density range (g/cm^3)	WDPT (s)	Classification
	WR-20/30-0	10:0		1.53-1.6	<5	Wettable
Ottawa	WR-20/30-1	9:1	0.2, 0.5, 1, 2, 3, 4,	1.58-1.63	50	Slightly water repellent
20/30 sand	WR-20/30-2	8:2	5, 6, 7, 8	1.59-1.66	120	Strongly water repellent
	WR-20/30-3	0:10		1.64-1.7	>3600	Extremely water repellent
	WR-50/70-0	10:0		1.44-1.54	<5	Wettable
Ottawa	WR-50/70-1	9:1	0.2, 0.5, 1, 2, 3, 4,	1.54-1.61	400	Strongly water repellent
50/70 sand	WR-50/70-2	8:2	5, 6, 7, 8, 9, 10,	1.56-1.62	2985	Sever water repellent
	WR-50/70-3	0:10	11, 12, 13, 14	1.58-1.64	>3600	Extremely water repellent

† Mass ratio of wettable sand to extremely water-repellent sand.

Figure 4-1 presents the experimental setup of thermal conductivity measurements. The SH-1 dual-needle probe was inserted into the compaction mold and then connected to KD2 Pro thermal properties analyzer. The SH-1 probe has two needles with a length of 30 mm, a diameter of 1,3 mm, and a spacing of 6 mm. It can provide thermal conductivity measurement with an accuracy of ±10% from 0.2 to 2.0 W/(m·K) and ± 0.01 W/(m·K) from 0.01 to 0.2 W/(m·K). Diffusivities and Volumetric specific heat can be also measured with an accuracy of ±10% at conductivities above 0.1 W/(m·K). All experimental data were automatically recorded.

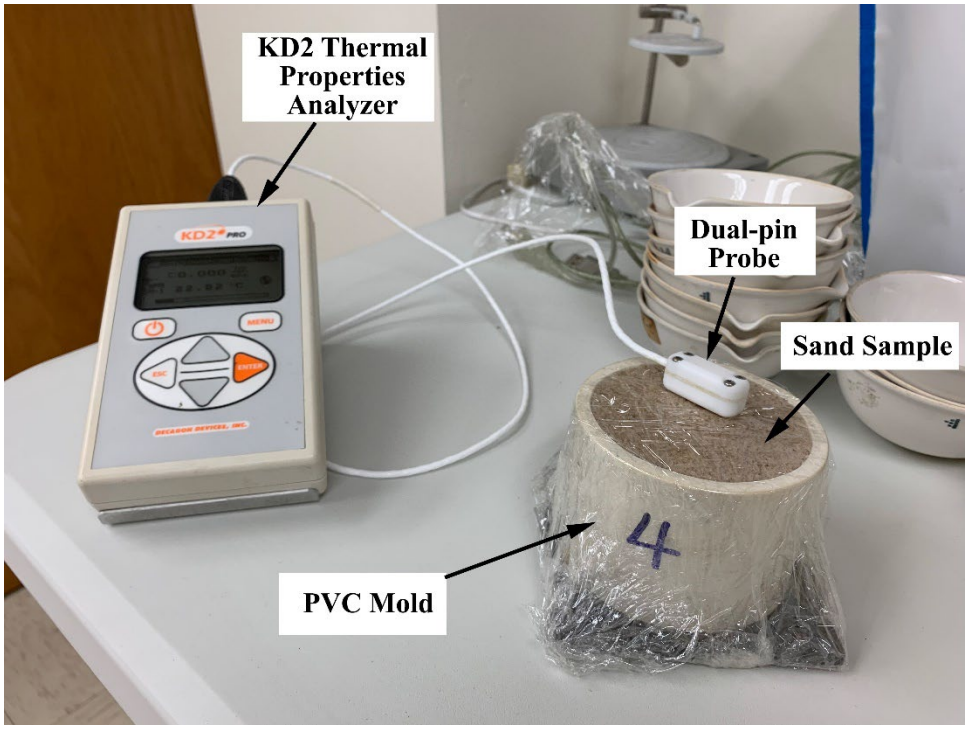

Figure 4- 1. Experimental setup of thermal conductivity measurement using KD2 Pro thermal properties measurement system.

4.3.2. Test procedure

The testing procedures for measuring soil thermal properties in the laboratory are illustrated in the following flowchart (Figure 4-2). After the data collection, the relationship between the degree of soil water repellency and soil thermal conductivity will be examined as well as thermal diffusivity and volumetric heat capacity. The influence of particle size on thermal conductivity will also be analyzed.

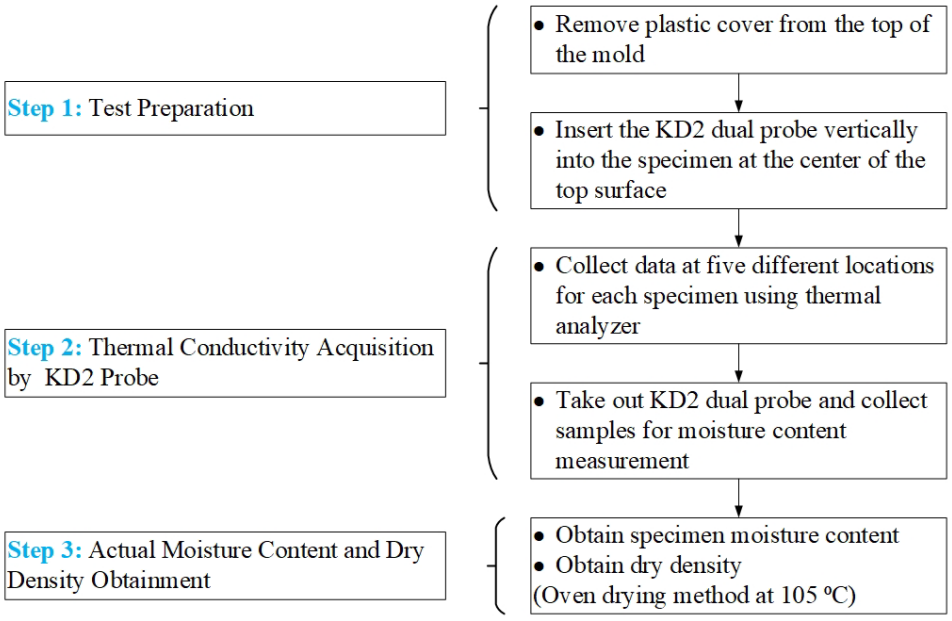

Figure 4- 2. Flowchart of the testing procedures for measuring soil thermal properties.

4.4. Results and Discussion

4.4.1. Thermal conductivity and degree of saturation

The relationship between thermal conductivity and degree of saturation, *S*, of both untreated and treated (wettable and water repellent) Ottawa 20/30 and 50/70 sands are presented in Figure 4-4. Thermal conductivity, *k*, of both untreated and treated sands was much higher in moist conditions than in dry conditions, meaning that it increased with a rising degree of saturation. In terms of untreated sands, Ottawa 50/70 sand showed larger thermal conductivities than Ottawa 20/30 sand when the degree of saturation was greater than 0.3. Compared with 20/30 sand, 50/70 sand had a smaller particle size, generating a higher specific surface area, therefore the water films and water bridges can easily form between sand particles. For mineral grain itself, the water films and water bridges may build heat flow barriers due to the water film coating on mineral grain surfaces (Midttomme and Roaldset, 1998). However, the water films and bridges, at the same time, filling pores between sand particles, facilitated the heat transfer process and increased thermal conductivity since water has higher thermal conductivity than air. Thermal resistance generated at the solid-water interface is less than that at the solid-air interface, therefore the existence of water between particles reduces the overall thermal resistance of sand samples.

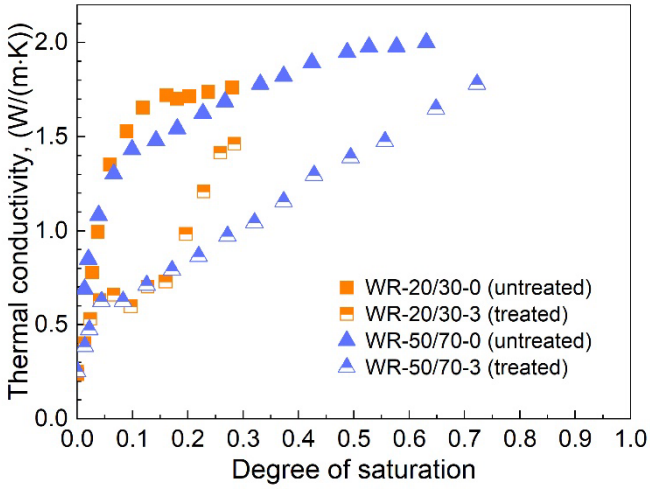

Figure 4- 3. Soil thermal conductivity as a function of degree of saturation as influenced by water repellency.

The DMDCS treatment significantly reduced sand thermal conductivity. Thermal conductivities of wettable and repellent sands differed from each other. The differences between the conductivities became larger with an increasing degree of saturation. The water repellent thin layer generated by DMDCS on sand grain surface hindered the formation of water film and water bridges between sand particles at lower moisture conditions. In addition, different patterns of thermal conductivity variation with saturation were found for hydrophobic samples (treated). All the water repellent samples displayed relatively constant thermal conductivity values in the region of the degree of saturation from 0.05 to 0.2. As the degree of saturation grew, the hydrophobic sands showed a fairly S-shape

increase path for thermal conductivity, which was sensitive to the particle size of samples. For treated coarse sand (WR-20/30-3), thermal conductivity accelerated rapidly as the degree of saturation increased. Water can easily penetrate into treated coarse sand to form water film or water bridges between sand particles, compared with treated fine sand (WR-50/70-3). The thermal conductivities of all water repellent samples can be projected to converge under saturated conditions.

4.4.2. Thermal conductivity and degree of water repellency

The influence of the degree of water repellency on sandy soils was systematically investigated in this section. The *k-S* relationship corresponding to the degree of water repellency was illustrated in Figure 4-5. The influence of water repellency depended on the degree of saturation, meaning that for samples with varying extent of water repellency, thermal conductivity in the dry conditions was not altered by water repellency. The critical degree of saturation value (S_r) at which the differences in thermal conductivity first occurred between samples of different repellencies was 0.041 and 0.022 for the Ottawa 20/30 sand and 50/70 sand, respectively. At a certain degree of saturation, larger than S_r, thermal conductivity decreased with the increase of water repellency. The wettable sand samples presented the largest thermal conductivities, while the completely hydrophobic samples had the lowest *k* values. When water contents near saturation, the

variations between samples with various degrees of water repellency appeared to be relatively small. Ottawa 20/30 sand samples were sensitive to the degree of water

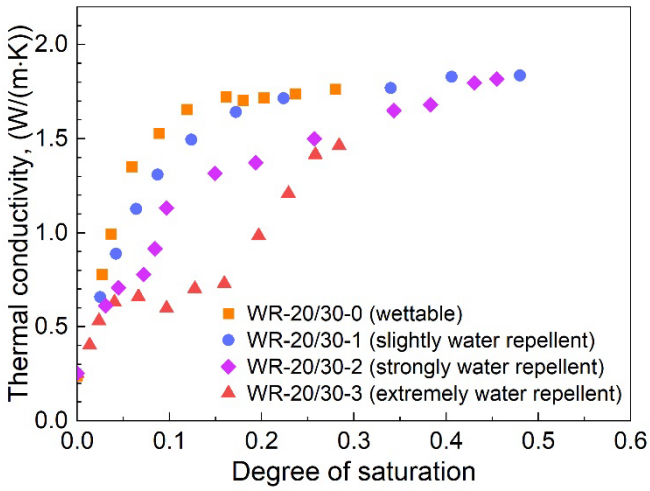

(a)

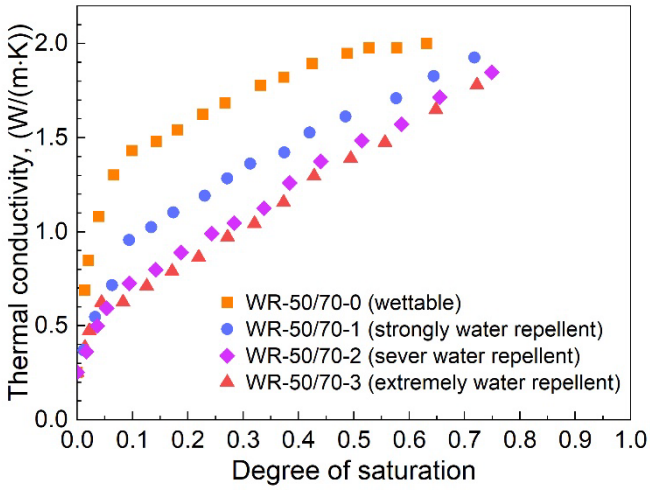

(b)

Figure 4- 4. Soil thermal conductivity as a function of degree of saturation as influenced by degree of water repellency, which varies from wettable to extremely water repellent.

repellency. Large variations occurred between samples with varying wettability when the degree of saturation ranged from 0.05 to 0.3. Sand wettability seemed to be susceptible to a small amount of water repellent particles, especially for fine-grained sand (Ottawa 50/70 sand). At the same level of water repellency, for example slightly water repellent, in terms of WR-50/70-1, the k value was significantly lower than wettable sand (WR-50/70-0). However, this enormous reduction was not obvious for coarse sand (Ottawa 20/30 sand).

The reduction of sand thermal conductivity caused by DMDCS treatment has been explicated in Section 4.4.1 by the effect of hydrophobicity on the formation of water films and bridges between sand particles. Little if any water films or bridges occurred on particle surfaces or between sand particles, when the sand degree of saturation was less than the critical value S_r. Subsequently, inconspicuous differences of thermal conductivity between wettable and water repellent sands were observed due to the minor impact of S on k values. As the degree of saturation surpassed S_r, water bridges between the water films on sand particles started to form, contributing remarkably to conductive heat transfer within sand samples. Soil hydrophobicity usually generates nonuniform water distribution within soils and hinders the formation of water bridges (Bachmann and van der Ploeg, 2002; Bauters et al., 2000). As a result, the hydrophobic sand presented much lower thermal conductivity compared to its wettable counterparts at a

particular degree of saturation. Back in the 1960s, Globus (1960) also discovered the reduction of flux of water vapor moving within layered porous materials stemmed from a layer of hydrophobized material placed in the middle of the corresponding non-hydrophobized material. Then he concluded that hydrophilization reduced the contribution of latent heat transfer to the thermal conductivity of water repellent medium.

4.4.3. Volumetric heat capacity and degree of saturation

Soil volumetric heat capacity *C* is defined as the change in the heat content of a unit bulk volume of soil per unit change in temperature (Hillel, 2004). *C* depends on the composition of the soil's solid phase, bulk density, and the soil's wetness. The value of *C* can be calculated by addition of the heat capacities of various constituents, as given by De Vries (1963).

$$C = \sum f_{si} C_{si} + f_w C_w + f_w C_w \tag{4.1}$$

Here, f presents the volume fraction of each phase: solid (s), water (w), and air (a).

In opposition to the thermal conductivities, the volumetric heat capacity of wettable sands agreed well with water repellent sands (Figure 4-6). Systematic differences of heat capacities between wettable and hydrophobic sands, compared with the thermal conductivities, were not noticed. The DMDCS treatment had trivial effects on sand volumetric heat capacity. The *C* values of both two types of

sands increased with an increasing degree of saturation. At high water content conditions, the air filled with pore space would be substituted with water. Since water possesses a higher thermal capacity than air, according to Eq. (4.1), with the same solid composition, the higher the water content was the greater volumetric heat capacity.

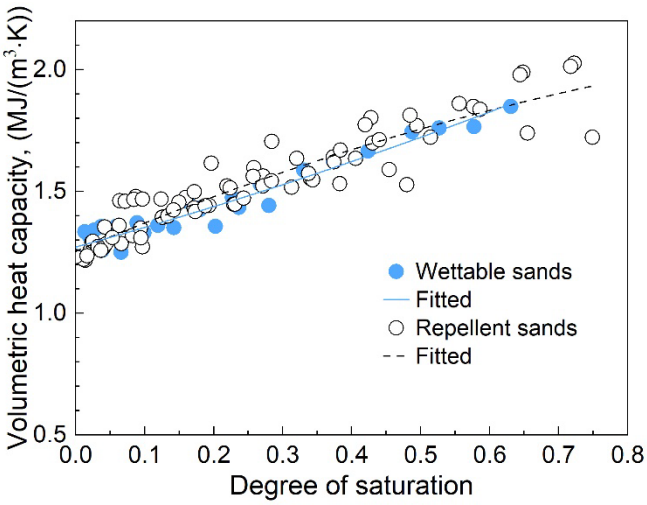

Figure 4- 5. Measured volumetric heat capacities of all wettable and water repellent sands.

4.5. Summary

Soil surface wettability and associated thermal behaviors have a high potential for engineering applications. In this chapter, thermal properties of sands with various degrees of surface hydrophobicity were investigated. The hypothesis has been verified that surface wettability, altering the particle-water interaction in porous media, has a vital effect on thermal conductivity. For unsaturated porous media, hydrophilic soils possess higher thermal conductivity due to the well-built water films and water bridges between solid particles, generating good paths for heat conduction. The water repellency hinders the formation of water bridges at the particle contacts and initiates nonuniform water distribution within soils, therefore resulting in poor pore fluid connectivity and low thermal conductivity. However, fewer impacts have been observed on the volumetric heat capacity of soils. This is because the heat capacity depends on the fraction of solid, liquid, and gas, but on the spatial arrangement of the phases.

CHAPTER 5. DEVELOPMENT OF A THERMAL CONDUCTIVITY MODEL FOR HYDROPHOBIC SANDS

5.1. Introduction

Apart from laboratory tests, the soil thermal conductivity prediction model has been conducted for a couple of decades. The first thermal conductivity model, derived from Maxwell's equations, was proposed by De Vries (1963), where the weighted average thermal conductivity of each phase of the soil matrix was considered. Since the early works of De Vries (1963) and Johansen (1975), numerous soil thermal conductivity predictive models have been proposed to investigate the impact of influence factors, including quartz content (Côté and Konrad, 2005b), porosity (Gangadhara Rao and Singh, 1999), degree of saturation (Donazzi et al., 1979), and organic matter (Balland and Arp, 2005), etc., on thermal conductivity. A thermal conductivity model was proposed by Lu et al. (2007) through a new k_r-S_r (thermal conductivity – degree of saturation) relationship across a wide range of soil moisture content; and the model was validated by performing a series of thermo-time domain reflectometry (TDR) tests on twelve soils ranging from sand, silt, to loam or clay loam. However, current soil conductivity predictive

models have been developed with the assumption that all soils are hydrophilic with a contact angle of 0 degrees.

Wildfire may cause convective airflow through the shallow subsurface, transporting combustion products and coating soil grain with organic vapors. The organic matter possibly produces hydrophobicity and decrease the effective thermal conductivity by sealing soil pores (DeBano, 2000). Campbell et al. (1994) extended the De Vries model (1963) to study the wildfire effects on soil thermal conductivities, which accounted for changes in both degree of saturation and temperature. Four fitting parameters, comprising of the mineral fraction, the cutoff for water content recirculation, the power for the recirculation function, and a shape factor, are involved in this model. Smits et al. (2016) utilized Campbell model to investigate changes in soil thermal conductivity after a wildfire or controlled burn and indicated that the model agreed well with laboratory measurements over the full range of water contents. Nevertheless, fitting parameters involved in this model need to be fitted to experimental data or predicted based on the physical properties of soils. The effects of water repellency on thermal conductivity are not clarified in the model.

This chapter presents the development and validation of a soil thermal conductivity prediction model for hydrophobic sands, considering the effects of degree of water repellency, degree of saturation, porosities, and temperature simultaneously. The model was validated using laboratory test results of

hydrophobic Ottawa 50/70 sand at different degrees of saturation with relatively constant room temperature. The model performance was also assessed via the comparison of predicted thermal conductivity with laboratory data from both other thermal conductivity measurements of water repellent sands from published literature (Dong, 2013).

5.2. Model Development

5.2.1. Framework of Campbell model

The Campbell model was modified from the De Vries (1963) model and proposed that soil effective thermal conductivity, k, can be determined from a volume-weighted sum of the k of the components of the mixture:

$$k = \frac{f_w x_w k_w + f_a x_a k_a + f_m x_m k_m}{f_w x_w + f_a x_a + f_m x_m} \tag{5.1}$$

where k is the effective soil thermal conductivity, k_w, k_a, and k_m are the effective thermal conductivity of water, air, and mineral, f_w, f_a, and f_m are empirically determined weighting factors of the components water, air, and mineral, and x_w, x_a, and x_m are the volume fractions of the components water, air, and mineral, respectively.

The volume fractions were assumed to be dependent on porosity and degree of saturation. The calculation can be expressed as:

$$x_w = n \cdot S_r \tag{5.3}$$

$$x_a = n \cdot (1 - S_r) \tag{5.4}$$

$$x_m = 1 - n \tag{5.5}$$

The thermal conductivity of mineral can be estimated if the mineral fraction and soil composition is known or fitted from experimental data. The thermal conductivity of water and dry air were adjusted for temperature by Campbell et al. (1994) using a quadratic function:

$$k_w = 0.554 + 2.24 \times 10^{-3} T - 9.87 \times 10^{-6} T^2 \tag{5.6}$$

$$k_{da} = 0.024 + 7.73 \times 10^{-5} T - 2.6 \times 10^{-8} T^2 \tag{5.7}$$

where T is the Celsius temperature. The apparent thermal conductivity of air is the sum of the dry conductivity, k_{da}, and a vapor term due to latent heat transfer. Since the laboratory tests were conducted under room temperature with an average value of 23 ºC. The vapor was assumed to have no effect on air thermal conductivity with sand samples. Therefore, the k_{da} was treated as the apparent thermal conductivity of air.

Weighting factors, f, were determined using a continuous function, applying over the full range of water contents. The expression is shown below.

$$f_i = \frac{1}{3}\left[\frac{2}{1+\left(\frac{k_i}{k^*}-1\right)g_i} + \frac{1}{1+\left(\frac{k_i}{k^*}-1\right)(1-2g_i)}\right] \tag{5.8}$$

where g_i are shaper factors of soil constituents ($i = w, a, m$). k^* a "fluid" thermal conductivity defined by Campbell et al. (1994):

$$k^* = k_a + \lambda_w(k_w - k_a) \tag{5.9}$$

where λ_w is an empirical weighting function given by:

$$\lambda_w = \frac{1}{1+\left(\frac{x_w}{x_{w0}}\right)^{-q}} \tag{5.10}$$

λ_w ranges from 0 in dry soil to 1 in saturated soil. The parameters x_{w0} and q are the cutoff for water content recirculation and the rapidity of the transition from air- to water-dominated conductivity, respectively. The transition between wet and dry soils is controlled by x_{w0}, which can be ideally predicted using the geometric mean particle diameter (d_g):

$$x_{w0} = 0.267{d_g}^{-0.2} \tag{5.11}$$

where d_g is in μm and x_{w0} is in m^3m^{-3}.

The term q is temperature dependent and defined as:

$$q = q_0\left(\frac{K}{303}\right)^2 \tag{5.12}$$

where q_0 is constant and can be obtained by fitting experimental data, and K is the Kelvin temperature of soils.

Generally, the shape factors of the soil control the magnitude of thermal conductivity across the entire range of water content. In the Campbell model, the shape factor of soil grains and water are assumed to be equal. Since the sum of shape factors is unit, only the shape factor of air needs to be fitted.

Campbell et al. (1994) claimed that only the four parameters are required to predict thermal conductivity. These are the mineral fraction, k_m, the cutoff for water content recirculation x_{w0}, the power for the recirculation function q, and a shape factor g_a. And the parameters can be fitted to experimental data.

5.2.2. Model modification

As summarized in the previous section, Campbell model needs four parameters to predict thermal conductivity, where most of the parameters are fitted to experimental data (Campbell et al., 1994; Smits et al., 2013). The objective of this study is to develop a thermal conductivity prediction model for hydrophobic sands. Therefore, several modifications based on Campbell model were conducted by considering the effect of the degree of water repellency. In addition, the four fitting parameters were reduced to two, by introducing new physical models.

5.2.2.1. Effect of degree of water repellency

The DMDCS treatment or other types of coating techniques induces a thin water repellent layer on sand particle surface. Particles are assumed to be wrapped

by a thin layer, as presented in Figure 5-1. As the induced PDMS has a much lower thermal conductivity (0.16 W/(m·K),(Zhou et al., 2022)) than quartz (7.69W/(m·K), (Chen, 2008)), the newly induced solid particles cannot be treated as pure quartz when calculating the thermal conductivity of mineral as illustrated in Eq. (5.1). Therefore, a geometric mean model was proposed to calculate thermal conductivity of solid particles in consideration of degree of water repellency:

$$k_m = k_{mineral}^{\phi_{mineral}} k_{coating}^{\phi_{coating}} \tag{5.13}$$

where ϕ_i is the volumetric fraction of each component (mineral and coating).

The effect of degree of hydrophobicity on the thermal conductivity of mineral can be simplified as volumetric fraction of coating. To accurately estimate $\phi_{coating}$, the thickness of the coating on particle surface needs to be calculated. Sand particles are assumed to be spheric and the PDMS coating is evenly distributed on the surface as shown in Figure 5-1. Then the thickness is calculated using Eq. (5.14) (Bardet et al., 2014):

$$w' = \frac{\rho_{PDMS}}{\rho_s}\left[\sum_{1}^{N} P_i\left(1 + \frac{t_i}{R_i}\right)^3 - 1\right] \tag{5.14}$$

where w' is the ratio of the mass of PDMS to that of soil particles, ρ_{PDMS} is the unit weight of PDMS (0.965 g/cm^3, (Matyjaszewski and Xia, 2001)), ρ_s is the unit weight of a sand particle, N_i is the number sand particles of radius R_i, P_i is the percentage by the weight corresponding to radius R_i, and t_i is the coating thickness.

In this study, the diameter of Ottawa 50/70 sand particle is simplified as d_{50}. The calculated coating thickness is approximately 4 μm. Then the volume of the coated sand particle can be obtained. The volume fraction of PDMS coating can be calculated.

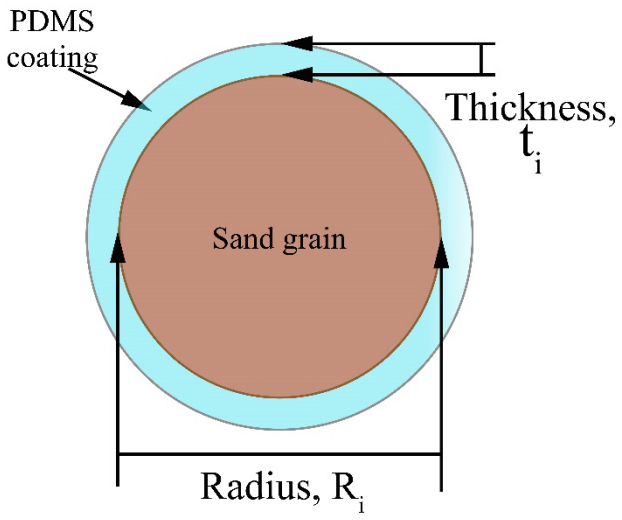

Figure 5- 1. Schematic of sand grain with a spherical PDMS coating.

5.2.2.2. Calculation of x_{w0}

The parameter, x_{w0}, affects the soil thermal conductivity at the transition between the pendular and hydration regimes. The empirical estimation of x_{w0} was developed by Campbell et al. based on the geometric mean particle diameter, d_g, as shown in Eq. (5.11). However, the calculation of d_g was not given. This section

introduces one estimation method to the model for calculating d_g for spherical sand particles. The determination of d_g can be expressed as (Luttrell, 1955):

$$d_g = \sum_{1}^{y} X \times d_{gm} \tag{5.15}$$

where d_g is geometric mean particle diameter, y is the number of sieved components in the solid's mixture, X is the weight fraction of closely screened material. $d_{gm} = \sqrt{d_1 \times d_2}$ is the geometric mean diameter of component retained between adjacent sieves having aperture sizes d_1 and d_2.

Substituting Eq. (5.15) into Eq. (5.11), the new x_{w0} for spherical sands can be calculated as:

$$x_{w0} = 0.267\left(\sum_{1}^{y} X \times d_{gm}\right)^{-0.2} \tag{5.16}$$

5.2.2.3. Shape factors g_i

The shape factors involved in Campbell model include the shape factor of soil grains, water particles, and air-filled pores. Generally, the shape factor of soil grains (g_s) varies from 0.0 (platy structure) to 0.333 (spheres), where for sandy grains, the value of g_s is approximately 0.144 (Tarnawski et al., 2021). In this study, it is assumed that water particles have the same shape factor as solid grains, meaning that $g_w = g_s = 0.144$. The shape factor of air-filled pores, g_a, needs to

be fitted to experimental data. The value of g_a ranges from 0.013 to 0.333 (Vries, 1963).

5.2.2.4. Thermal conductivity prediction model for hydrophobic sands

Based on the modification discussed in the aforementioned section, the modified thermal conductivity prediction model for hydrophobic sands is expressed as:

$$k_{hs} = \frac{f_w x_w k_w + f_a x_a k_a + f_m x_m \left(k_{mineral}^{\phi_{mineral}} k_{coating}^{\phi_{coating}}\right)}{f_w x_w + f_a x_a + f_m x_m} \tag{5.17}$$

where the volume fractions (x_i) of the components water, air, and mineral, respectively, keep the same as Campbell model. The calculation of f_i also remains the same except for the estimation of x_{w0}, which is obtained from Eq. (5.16). The shape factors of sand grains and water particles are set to be 0.144. The shape factor, g_a, and the power for the recirculation function, q_0, need to be fitted to experimental data

5.2.3. Model validation

Since few databased can be found in literature in terms of the behavior of hydrophobic sand thermal conductivity, the prediction model was validated only using the present experimental data (Section 4.4.2) of effective thermal conductivity as a function of degree of saturation. The comparison between

predicted thermal conductivity and measured data was illustrated in Figure 5-2, with input parameters listed in Table 5-1. The effective thermal conductivity of the mineral fraction, k_m, was calculated using a geometric function, Eq. (5.13). The volumetric fraction of PDMS coating represented the effects of degree of water repellency. The cutoff for water content recirculation, x_{w0}, which controls the transition of unsaturated and saturated regions, was obtained from Eq. (5.19) associated with the calculation of geometric mean particle diameter of sand samples. As the shapes of all hydrophobic sample curves were similar (Figure 5-2), the value of x_{w0} for all samples remained the same. The parameters, g_a and q_0, were obtained by fitting to experimental data.

Table 5- 1. Parameters for improved prediction model for hydrophobic sand samples with various degrees of water repellency.

Sand samples	$\boldsymbol{\phi_{coating}}$	$\boldsymbol{k_m}$ **(W/(m·K))**	$\boldsymbol{d_g}$ **(μm)**	$\boldsymbol{x_{w0}}$	$\boldsymbol{g_a}$	$\boldsymbol{q_0}$	**RMSE**
WR-20/30-1	0.003	7.5	642.62	0.073	0.114	0.772	0.04
WR-20/30-2	0.006	7.59	642.62	0.073	0.059	0.842	0.09
WR-20/30-3	0.033	6.78	642.62	0.073	0.084	1.31	0.12
WR-50/70-1	0.007	7.48	249.17	0.088	0.053	1.012	0.03
WR-50/70-2	0.014	7.27	249.17	0.088	0.108	0.811	0.05
WR-50/70-3	0.070	5.86	249.17	0.088	0.061	1.026	0.04

The RMSE analysis was conducted to evaluate the performance of the improved prediction model, using Eq. (5.18). The RMSE values for the predicted and experimental data suggest that the estimated effective thermal conductivity values were in good agreement with the measured values, except for WR-20/30-3. Compared with other samples, the thermal conductivity curve of WR-20/30-3 has a region where the thermal conductivity remains constant with the increase of degree of saturation. This phenomenon indicates that cavitation is most pronounced due to the surface treatment and large particle size, so much that soil void is mostly occupied by air. The new model doesn't consider the effects of cavitation of water in soil. Further investigation needs to be conducted. In addition, RMSE values regarding fine sand samples are small and keep relatively stable, indicating the new model is more suitable for fine sands. Overall, from the comparison between predicted results and measured data, the improved thermal conductivity prediction model can be used to estimate the effective thermal conductivity of hydrophobic sands.

$$RMSE = \sqrt{\frac{1}{n}\sum_{1}^{n}\left(\frac{k_{exp} - k_{model}}{k_{exp}}\right)^2} \tag{5.18}$$

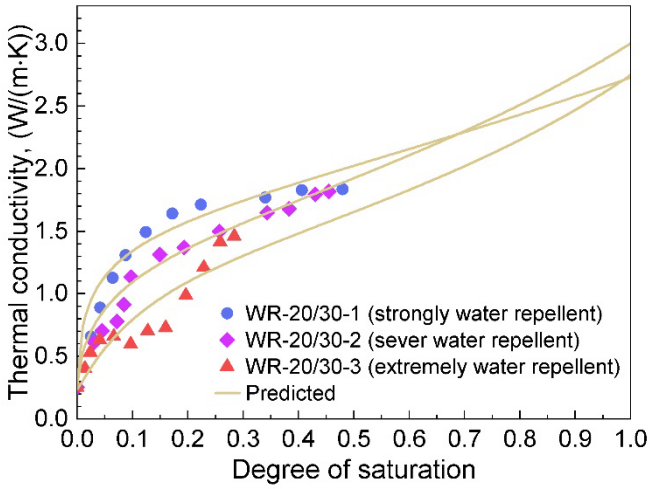

(a)

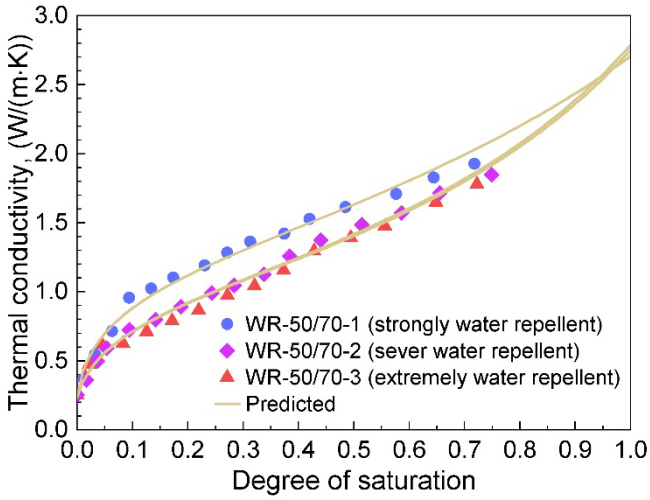

(b)

Figure 5- 2. Comparison of the effective thermal conductivity between the experimental data and predicted data from improved Campbell model considering the effects of degree of water repellency: (a) Ottawa 20/30 sand, (b) Ottawa 50/70 sand.

5.2.4. Estimation of thermal conductivity over the full range of degree of saturation

Figure 5-3 presents the comparisons of predicted thermal conductivity with measured values of hydrophobized Ottawa 20/30 sand from Dong's (2013) study. Since volume fraction of coating was not provided in the study, the measured data with the void ratio of 0.6 was utilized to perform parameter fitting to obtain the thermal conductivity of mineral and coating mixture, k_m. The obtained value of k_m is 6.33 W/(m·K). Then k_m was applied to the prediction of thermal conductivity for sand samples with void ratios of 0.56 and 0.58. Parameters used in the prediction were summarized in Table 5-2. The predicted thermal conductivity was found to be in good agreement with the measured values when degree of saturation is less than 0.4. The model overestimated thermal conductivity when Sr ranges from 0.4 to 0.8, indicating that calibration of four parameters needs to perform. Without calibration, the new continuum thermal conductivity prediction model can only be used for prediction of thermal conductivity for hydrophobic coarse sand with low degree of saturation.

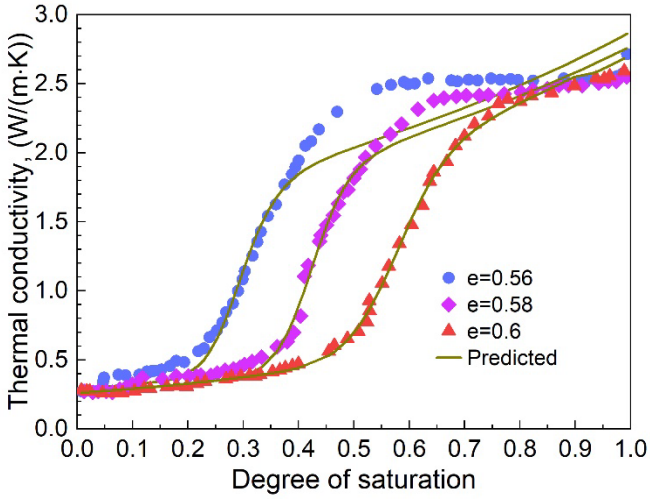

Figure 5- 3. Comparison of the effective thermal conductivity between the experimental data and predicted data from Dong's (2013) study.

Table 5- 2. Parameters for prediction model for hydrophobic sand from Dong's (2013) study.

Void ratio	$\phi_{coating}$	k_m (W/(m·K))	x_{w0}	g_a	q_0	RMSE
0.56		6.33	0.119	0.116	8.57	0.32
0.58	N/A	6.33	0.168	0.129	12.36	0.18
0.60		6.33	0.235	0.118	12.86	0.07

5.3. Summary

Soil thermal conductivity is of great importance in the design of geothermal energy piles and borehole thermal energy storage, etc. Some of the energy systems are generally shallowly buried, where part of soils interacted with the system may be water repellent due to influences of contaminations and plant roots. In this chapter, a new soil thermal conductivity model was proposed based on laboratory tests on hydrophobic sands. The major conclusions of this chapter were drawn below.

Current thermal conductivity prediction models merely consider the effect of hydrophobization on soil thermal conductivity. A new thermal conductivity model was developed based on Campbell model by considering the effect of degree of water repellency. The effects on degree of water repellency were introduced to the new model and can be calculated based on the hydrophobic sand texture. The cutoff for water content recirculation, x_{w0}, which is a parameter controlling the transition of unsaturated and saturated regions, was obtained associated with the calculation of geometric mean particle diameter of sand samples. The other two parameters were acquired by empirical fits to experimental data. The model was validated by experimental data, which fills the gap in predicting thermal conductivity for hydrophobic sands. But it should be noted that the model validation for thermal conductivity prediction might not be adequate due to the lack of thermal

conductivity data of water repellent sands in previous literature, yet the predicted thermal conductivities were still found to be in good agreement with experimental data. The new continuum thermal conductivity prediction model needs parameter calibration when estimating thermal conductivity with full range of degree of saturation.

CHAPTER 6. CONCLUSIONS AND RECOMMENDATIONS

6.1. Conclusions

Chemical treatment techniques have been implemented to perform soil modification to simulate the natural water repellent soils induced by either wildfire or contaminations et al. This research majorly contributed to a fundamental understanding of thermal properties in unsaturated soils with various degrees of water repellency, including thermal conductivity and volumetric heat capacity. Further, a new continuum thermal conductivity prediction model has been developed by considering the impacts of water repellency.

The most important conclusions from this study are summarized as follows:

Surface modification: DMDCS (dimethyldichlorosilane) treatment has been proved to be an efficient material to induce surface hydrophobization of geomaterials, such as sand particles. The generated PDMS (polydimethylsiloxane), a product of DMDCS treatment, on the sand surface is with strong bonding and exceptional quality.

Thermal behaviors: the hypothesis has been verified that surface wettability, altering the particle-water interaction in porous media, has an important impact on

thermal conductivity. For unsaturated hydrophilic soils, the well-built water films and water bridges between solid particles, generating good paths for heat conduction, result in higher thermal conductivity. The water repellency hinders the formation of water bridges at the particle contacts and initiates nonuniform water distribution within soils, therefore resulting in poor pore fluid connectivity and low thermal conductivity even at a high degree of saturation for hydrophobic soils. Since heat capacity depends on the fraction of solid, liquid, and gas, but on the spatial arrangement of the phases, water repellency has fewer impacts on the volumetric heat capacity of soils.

Thermal conductivity prediction model: A new continuum soil thermal conductivity was developed based on Campbell model (1994), which fills the gap of predicting thermal conductivity for hydrophobic sands. The new model considered the effects of the degree of water repellency, degree of saturation, porosities, and temperature simultaneously on the thermal conductivity. Validation was performed that the predicted thermal conductivities were found to be in good agreement with experimental data. The new continuum thermal conductivity prediction model needs parameter calibration when estimating thermal conductivity with full range of degree of saturation.

6.2. Recommendations and Future Research

I suggest the following areas of further study:

- Investigation of the effects of degradation of hydrophobicity induced by UV, solvent exposure, and biological activities to thermal behaviors.
- Further evaluation on the effects of particle size on thermal and hydraulic behaviors of water repellent soils, especially the effects on unsaturated permeability.
- Extension of the new soil thermal conductivity model to a unified model for all types of hydrophobic soils.
- Examination of the relationship between the degree of water repellency and small-strain stiffness of soils (shear wave and frequency).
- Evaluation of the relationship between SWCC and thermal conductivity of hydrophobic sands.
- Advanced study on coupled thermo-hydro behaviors for heterogeneous and anisotropic particulate materials considering the effects of surface wettability.

REFERENCE

Abu-Hamdeh, N.H., 2003. Thermal Properties of Soils as affected by Density and Water Content. Biosystems Engineering 86 (1), 97–102. doi:10.1016/S1537-5110(03)00112-0.

Ahmed, M.E., van Geel, P.J., 2009. Potential concerns related to using octadecyltrichlorosilane (OTS) in rendering soils and porous ceramics hydrophobic. Journal of contaminant hydrology 110 (1-2), 22–33. doi:10.1016/j.jconhyd.2009.07.007.

Almendros, G., Martín, F., González-Vila, F.J., 1988. Effects of fire on humic and lipid fractions in a Dystric Xerochrept in Spain. Geoderma 42 (2), 115–127. doi:10.1016/0016-7061(88)90028-6.

AlRatrout, A., Blunt, M.J., Bijeljic, B., 2018. Wettability in complex porous materials, the mixed-wet state, and its relationship to surface roughness. Proceedings of the National Academy of Sciences of the United States of America 115 (36), 8901–8906. doi:10.1073/pnas.1803734115.

ASTM D854, 2014. Test Methods for Specific Gravity of Soil Solids by Water Pycnometer. ASTM International, West Conshohocken, PA. doi:10.1520/D0854-14.

Bachmann, J., Ellies, A., Hartge, K., 2000. Development and application of a new sessile drop contact angle method to assess soil water repellency. Journal of Hydrology 231-232, 66–75. doi:10.1016/S0022-1694(00)00184-0.

Bachmann, J., Horton, R., Ren, T., van der Ploeg, R.R., 2001. Comparison of the thermal properties of four wettable and four water-repellent soils. Soil Sci. Soc. Am. J. 65 (6), 1675–1679. doi:10.2136/sssaj2001.1675.

Bachmann, J., van der Ploeg, R.R., 2002. A review on recent developments in soil water retention theory: interfacial tension and temperature effects. Zeitschrift für Pflanzenernährung und Bodenkunde 165 (4), 468. doi:10.1002/1522-2624(200208)165:4<468:aid-jpln468>3.0.co;2-g.

Bachmann, J., Woche, S.K., Goebel, M.-O., Kirkham, M.B., Horton, R., 2003. Extended methodology for determining wetting properties of porous media. Water Resour. Res. 39 (12). doi:10.1029/2003WR002143.

Balland, V., Arp, P.A., 2005. Modeling soil thermal conductivities over a wide range of conditions. Journal of Environmental Engineering and Science 4 (6), 549–558. doi:10.1139/s05-007.

Bardet, J.-P., Jesmani, M., Jabbari, N., 2014. Permeability and compressibility of wax-coated sands. Géotechnique 64 (5), 341–350. doi:10.1680/geot.13.P.118.

Bauters, T., Steenhuis, T., DiCarlo, D., Nieber, J., Dekker, L., Ritsema, C., Parlange, J.-Y., Haverkamp, R., 2000. Physics of water repellent soils. Journal of Hydrology 231-232, 233–243. doi:10.1016/S0022-1694(00)00197-9.

Blossey, R., 2003. Self-cleaning surfaces--virtual realities. Nature Materials 2 (5), 301–306. doi:10.1038/nmat856.

Boggs, S.A., 1982. Underground cable thermal backfill. Pergamon Press, Toronto, New York.

Bornemisza, E., 1964. Wettability of soils in relation to their physico-chemical properties. Dissertation, Gainesville, Florida, USA.

Bourrié, G. (Ed.), 2019. Soils as a Key Component of the Critical Zone 3 - Soils and Water Circulation: Soils and water circulation, 1st ed. ed. John Wiley & Sons, Inc, [Place of publication not identified], 1 online resource.

Brandon, T.L., Mitchell, J.K., Cameron, J.T., 1989. Thermal Instability in Buried Cable Backfills. J. Geotech. Engrg. 115 (1), 38–55. doi:10.1061/(ASCE)0733-9410(1989)115:1(38).

Buczko, U., Bens, O., 2006. Assessing Soil Hydrophobicity and Its Variability through the Soil Profile Using Two Different Methods. Soil Sci. Soc. Am. J. 70 (3), 718–727. doi:10.2136/sssaj2005.0183.

Campbell, G.S., Jungbauer, J.D., Bidlake, W.R., Hungerford, R.D., 1994. PREDICTING THE EFFECT OF TEMPERATURE ON SOIL THERMAL CONDUCTIVITY. Soil Science 158 (5), 307.

Carrillo, M.L.K., Yates, S.R., Letey, J., 1999. Measurement of Initial Soil-Water Contact Angle of Water Repellent Soils. Soil Sci. Soc. Am. J. 63 (3), 433–436. doi:10.2136/sssaj1999.03615995006300030002x.

Cassie, A., Baxter, S., 1945. Large contact angles of plant and animal surfaces. Nature communications 155 (3923), 21–22.

Cassie, A.B.D., Baxter, S., 1944. Wettability of porous surfaces. Trans. Faraday Soc. 40, 546. doi:10.1039/tf9444000546.

Chan, C.S.H., Lourenço, S.D.N., 2016. Comparison of three silane compounds to impart water repellency in an industrial sand. Géotechnique Letters 6 (4), 263–266. doi:10.1680/jgele.16.00097.

Chen, S.X., 2008. Thermal conductivity of sands. Heat Mass Transfer 44 (10), 1241–1246. doi:10.1007/s00231-007-0357-1.

Côté, J., Konrad, J.-M., 2005a. A generalized thermal conductivity model for soils and construction materials. Can. Geotech. J. 42 (2), 443–458. doi:10.1139/t04-106.

Côté, J., Konrad, J.-M., 2005b. Thermal conductivity of base-course materials. Can. Geotech. J. 42 (1), 61–78. doi:10.1139/t04-081.

D. Y. Kwok, T. Gietzelt, K. Grundke, H.-J. Jacobasch, and A. W. Neumann, 1997. Contact Angle Measurements and Contact Angle Interpretation. 1. Contact Angle Measurements by Axisymmetric Drop Shape Analysis and a Goniometer Sessile Drop Technique. Langmuir 13, 2880–2894.

D.Y.Kwok, A.W. Neumann, 1999. Contact angle measurement and contact angle interpretation. Advances in Colloid and Interface Science 81, 167–249.

Daniel, N.R., Uddin, S.M., Harper, R.J., Henry, D.J., 2019. Soil water repellency: A molecular-level perspective of a global environmental phenomenon. Geoderma 338, 56–66. doi:10.1016/j.geoderma.2018.11.039.

DeBano, L., 2000. Water repellency in soils: a historical overview. Journal of Hydrology 231-232, 4–32. doi:10.1016/S0022-1694(00)00180-3.

Dekker, L.W., Ritsema, C.J., Oostindie, K., Boersma, O.H., 1998. EFFECT OF DRYING TEMPERATURE ON THE SEVERITY OF SOIL WATER REPELLENCY. Soil Science 163 (10), 780–796. doi:10.1097/00010694-199810000-00002.

Dell'Avanzi, E., Guizelini, A.P., Da Silva, W.R., Nocko, L.M., Buzzi, O., 2010. Potential use of induced soil-water repellency techniques to improve the performance of landfill's alternative final cover systems (pp. 461-466). CRC Press, Boca Raton, FL.

DeVera, A.L., Strieder, W., 1977. Upper and lower bounds on the thermal conductivity of a random, two-phase material. J. Phys. Chem. 81 (18), 1783–1790. doi:10.1021/j100533a014.

Doerr, S., Thomas, A., 2000. The role of soil moisture in controlling water repellency: new evidence from forest soils in Portugal. Journal of Hydrology 231-232, 134–147. doi:10.1016/S0022-1694(00)00190-6.

Doerr, S.H., 1998. On standardizing the ‘Water Drop Penetration Time’ and the ‘Molarity of an Ethanol Droplet’ techniques to classify soil hydrophobicity: A

case study using medium textured soils. Earth Surf. Process. Landforms 23 (7), 663–668. doi:10.1002/(SICI)1096-9837(199807)23:7<663:AID-ESP909>3.0.CO;2-6.

Doerr, S.H., Llewellyn, C.T., Douglas, P., Morley, C.P., Mainwaring, K.A., Haskins, C., Johnsey, L., Ritsema, C.J., Stagnitti, F., Allinson, G., Ferreira, D., Keizer, J.J., Ziogas, A.K., Diamantis, J., 2005. Extraction of compounds associated with water repellency in sandy soils of different origin. Soil Res. 43 (3), 225. doi:10.1071/SR04091.

Doerr, S.H., Shakesby, R.A., Walsh, R., 2000. Soil water repellency: its causes, characteristics and hydro-geomorphological significance. Earth-Science Reviews 51 (1-4), 33–65. doi:10.1016/S0012-8252(00)00011-8.

Donazzi, F., Occhini, E., Seppi, A., 1979. Soil thermal and hydrological characteristics in designing underground cables. Proc. Inst. Electr. Eng. UK 126 (6), 506. doi:10.1049/piee.1979.0119.

Dong, Y., 2013. Engineered Soil with Thermally Controlled Wettability. Dissertation.

Dong, Y., McCartney, J.S., Lu, N., 2015. Critical Review of Thermal Conductivity Models for Unsaturated Soils. Geotech Geol Eng 33 (2), 207–221. doi:10.1007/s10706-015-9843-2.

Dorrer, C., Rühe, J., 2008. Wetting of Silicon Nanograss: From Superhydrophilic to Superhydrophobic Surfaces. Adv. Mater. 20 (1), 159–163. doi:10.1002/adma.200701140.

Fadejev, J., Simson, R., Kurnitski, J., Haghighat, F., 2017. A review on energy piles design, sizing and modelling. Energy 122, 390–407. doi:10.1016/j.energy.2017.01.097.

Farouki, O.T., 1981. Thermal Properties of Soils. Defense Technical Information Center, Fort Belvoir, VA.

Feyyisa, J.L., Daniels, J.L., Pando, M.A., Ogunro, V.O., 2019. Relationship between breakthrough pressure and contact angle for organo-silane treated coal fly ash. Environmental Technology & Innovation 14, 100332. doi:10.1016/j.eti.2019.100332.

Franco, C., Clarke, P., Tate, M., Oades, J., 2000. Hydrophobic properties and chemical characterisation of natural water repellent materials in Australian sands. Journal of Hydrology 231-232, 47–58. doi:10.1016/S0022-1694(00)00182-7.

Gangadhara Rao, M., Singh, D.N., 1999. A generalized relationship to estimate thermal resistivity of soils. Can. Geotech. J. 36 (4), 767–773. doi:10.1139/t99-037.

Gao, N., Yan, Y., 2009. Modeling Superhydrophobic Contact Angles and Wetting Transition. J Bionic Eng 6 (4), 335–340. doi:10.1016/S1672-6529(08)60135-3.

Gilboa, A., Bachmann, J., Woche, S.K., Chen, Y., 2006. Applicability of Interfacial Theories of Surface Tension to Water-Repellent Soils. Soil Sci. Soc. Am. J. 70 (5), 1417–1429. doi:10.2136/sssaj2005.0033.

Globus, A.M., 1960. Experimental study of phase composition of soil and ground moisture moving under the influence of temperature gradient [in Russian]. Doclady.

Goebel, M.-O., Woche, S.K., Bachmann, J., Lamparter, A., Fischer, W.R., 2007. Significance of Wettability-Induced Changes in Microscopic Water Distribution for Soil Organic Matter Decomposition. Soil Sci. Soc. Am. J. 71 (5), 1593–1599. doi:10.2136/sssaj2006.0192.

Gori, F., Corasaniti, S., 2002. Theoretical Prediction of the Soil Thermal Conductivity at Moderately High Temperatures. Journal of Heat Transfer 124 (6), 1001–1008. doi:10.1115/1.1513573.

Haigh, S.K., 2012. Thermal conductivity of sands. Géotechnique 62 (7), 617–625. doi:10.1680/geot.11.P.043.

Hillel, D., 2004. Introduction to environmental soil physics. Elsevier Academic Press, Amsterdam, Boston, 494 pp.

Horton, R., Wierngа, P.J., 1984. THE EFFECT OF COLUMN WETTING ON SOIL THERMAL CONDUCTIVITY1. Soil Science 138 (2), 102–108. doi:10.1097/00010694-198408000-00002.

Houston, S.L., Dye, H.B., Lingnau, B., Houston, W.N., 2015. Thermally-Induced Settlements for Heat Generating Structures on Unsaturated Soils. Geotech Geol Eng 33 (2), 307–319. doi:10.1007/s10706-014-9812-1.

J. Bachmann, 2000. Development and application of a new sessile drop contact angle method to assess soil water repellency. Journal of Hydrology 231-232, 66–75.

Johansen, O., 1975. Thermal conductivity of soils. Ph.D. thesis, Trondheim, Norway. Cold Regions Research and Engineering Laboratory Draft Translation 637, 1977, ADA 044002.

Johnson, R.E., Dettre, R.H., 1964. Contact Angle Hysteresis, in: Fowkes, F.M. (Ed.), Contact Angle, Wettability, and Adhesion, vol. 43. AMERICAN CHEMICAL SOCIETY, WASHINGTON, D.C., pp. 112–135.

Ju, Z., Ren, T., Horton, R., 2008. INFLUENCES OF DICHLORODIMETHYLSILANE TREATMENT ON SOIL HYDROPHOBICITY, THERMAL CONDUCTIVITY, AND ELECTRICAL CONDUCTIVITY. Soil Science 173 (7), 425–432. doi:10.1097/SS.0b013e31817b6658.

Kawamoto, K., Moldrup, P., Komatsu, T., Jonge, L.W. de, Oda, M., 2007. Water Repellency of Aggregate Size Fractions of a Volcanic Ash Soil. Soil Sci. Soc. Am. J. 71 (6), 1658–1666. doi:10.2136/sssaj2006.0284.

Kersten, M.S., 1949. Laboratory research for the determination of the thermal properties of soils: Technical Report 23. Research Laboratory Investigations, Engineering Experiment Station, University of Minnesota, Minneapolis, Minn, 234 pp.

Kimball, B.A., Jackson, R.D., Reginato, R.J., Nakayama, F.S., Idso, S.B., 1976. Comparison of Field-measured and Calculated Soil-heat Fluxes. Soil Sci. Soc. Am. J. 40 (1), 18–25. doi:10.2136/sssaj1976.03615995004000010010x.

King, P.M., 1981. Comparison of methods for measuring severity of water repellence of sandy soils and assessment of some factors that affect its measurement. Soil Res. 19 (3), 275. doi:10.1071/SR9810275.

Laloui, L., Rotta Loria, A.F., 2019. Analysis and design of energy geostructures: Theoretical essentials and practical application / Lyesse Laloui, Alessandro F. Rotta Loria. Academic Press, Amsterdam.

Lee, C., Yang, H.-J., Yun, T.S., Choi, Y., Yang, S., 2015. Water-Entry Pressure and Friction Angle in an Artificially Synthesized Water-Repellent Silty Soil. Vadose zone j. 14 (4), vzj2014.08.0106. doi:10.2136/vzj2014.08.0106.

Leelamanie, D.A.L., Karube, J., Yoshida, A., 2008. Characterizing water repellency indices: Contact angle and water drop penetration time of

hydrophobized sand. Soil Science and Plant Nutrition 54 (2), 179–187. doi:10.1111/j.1747-0765.2007.00232.x.

Letey, J., Carrillo, M., Pang, X., 2000. Approaches to characterize the degree of water repellency. Journal of Hydrology 231-232, 61–65. doi:10.1016/S0022-1694(00)00183-9.

Li, B., Han, Z., Hu, H., Bai, C., 2020. Study on the effect of groundwater flow on the identification of thermal properties of soils. Renewable Energy 147, 2688–2695. doi:10.1016/j.renene.2018.06.108.

Lin, H., 2020. Experimental investigation on the durability of hydrophobized soils: HKU Theses Online (HKUTO). Doctoral.

Liu, D., Lourenço, S.D.N., Yang, J., Zhou, Z., Leung, A.K., 2020. Critical state of polymer-coated sands. Géotechnique 70 (9), 839–841. doi:10.1680/jgeot.19.D.001.

Lourenço, S., Jones, N., Morley, C., Doerr, S.H., Bryant, R., 2015. Hysteresis in the Soil Water Retention of a Sand-Clay Mixture with Contact Angles Lower than Ninety Degrees. Vadose zone j. 14 (7), vzj2014.07.0088. doi:10.2136/vzj2014.07.0088.

Lourenço, S.D.N., Saulick, Y., Zheng, S., Kang, H., Liu, D., Lin, H., Yao, T., 2018. Soil wettability in ground engineering: fundamentals, methods, and applications. Acta Geotech. 13 (1), 1–14. doi:10.1007/s11440-017-0570-0.

Lu, S., Ren, T., Gong, Y., Horton, R., 2007. An Improved Model for Predicting Soil Thermal Conductivity from Water Content at Room Temperature. Soil Sci. Soc. Am. J. 71 (1), 8–14. doi:10.2136/sssaj2006.0041.

Luttrell, R.S., 1955. Determination of the mean particle diameter, particle density, and fraction voids of Ottawa sand. Bachelor.

Mainwaring, K., Hallin, I.L., Douglas, P., Doerr, S.H., Morley, C.P., 2013. The role of naturally occurring organic compounds in causing soil water repellency. Eur J Soil Sci 64 (5), 667–680. doi:10.1111/ejss.12078.

Marmur, A., 2003. Wetting on Hydrophobic Rough Surfaces: To Be Heterogeneous or Not To Be? Langmuir 19 (20), 8343–8348. doi:10.1021/la0344682.

Ma'shum, M., Tate, M., Jones, G.P., Oades, J.M., 1988. Extraction and characterization of water-repellent materials from Australian soils. Journal of Soil Science 39 (1), 99–110. doi:10.1111/j.1365-2389.1988.tb01198.x.

Matyjaszewski, K., Xia, J., 2001. Atom transfer radical polymerization. Chemical reviews 101 (9), 2921–2990. doi:10.1021/cr940534g. https://pubs.acs.org/doi/full/10.1021/cr940534g.

Midttomme, K., Roaldset, E., 1998. The effect of grain size on thermal conductivity of quartz sands and silts. Petroleum Geoscience 4 (2), 165–172. doi:10.1144/petgeo.4.2.165.

Moody, D.R., Schlossberg, M.J., 2010. Soil Water Repellency Index Prediction Using the Molarity of Ethanol Droplet Test. Vadose zone j. 9 (4), 1046–1051. doi:10.2136/vzj2009.0119.

Morley, C.P., Mainwaring, K.A., Doerr, S.H., Douglas, P., Llewellyn, C.T., Dekker, L.W., 2005a. Organic compounds at different depths in a sandy soil and their role in water repellency. Soil Res. 43 (3), 239. doi:10.1071/SR04094.

Morley, C.P., Mainwaring, K.A., Doerr, S.H., Douglas, P., Llewellyn, C.T., Dekker, L.W., 2005b. Organic compounds at different depths in a sandy soil and their role in water repellency. Soil Res. 43 (3), 239. doi:10.1071/SR04094.

Ng, S.H.Y., Lourenço, S.D.N., 2016. Conditions to induce water repellency in soils with dimethyldichlorosilane. Géotechnique 66 (5), 441–444. doi:10.1680/jgeot.15.T.025.

Oh, H., Tinjum, J.M., 2021. Comparison of Two Laboratory Methods for Measuring Soil Critical Temperature. Geotech. Test. J. 44 (2), 20190400. doi:10.1520/GTJ20190400.

Ojovan, M.I., Lee, W.E., Kalmykov, S.N., 2019. An introduction to nuclear waste immobilisation, Third edition / Michael I. Ojovan, William E. Lee, Stepan N. Kalmykov ed. Elsevier, Amsterdam.

Owen, M.J., 2001. Elastomers: Siloxane, in: Buschow, K.H.J. (Ed.), Encyclopedia of materials. Science and technology / edited by K.H. Jürgen Buschow … [et al.]. Elsevier, Amsterdam, London, pp. 2480–2482.

Ramé, E., 1997. The Interpretation of Dynamic Contact Angles Measured by the Wilhelmy Plate Method. Journal of colloid and interface science 185 (1), 245–251. doi:10.1006/jcis.1996.4589.

Ritsema, C.J., Dekker, L.W., 1996. Water repellency and its role in forming preferred flow paths in soils. Soil Res. 34 (4), 475–487. doi:10.1071/sr9960475.

Sass, J.H., Lachenbruch, A.H., Munroe, R.J., 1971. Thermal conductivity of rocks from measurements on fragments and its application to heat-flow determinations. J. Geophys. Res. 76 (14), 3391–3401. doi:10.1029/JB076i014p03391.

Saulick, Y., Lourenço, S., Baudet, B.A., 2017. A Semi-Automated Technique for Repeatable and Reproducible Contact Angle Measurements in Granular Materials using the Sessile Drop Method. Soil Sci. Soc. Am. J. 81 (2), 241–249. doi:10.2136/sssaj2016.04.0131.

Selker, J.S., Steenhuis, T.S., Parlange, J., 1991. Estimation of loading via fingered flow. Irrigation and drainage, 81–87.

Shakesby, R.A., Doerr, S.H., 2006. Wildfire as a hydrological and geomorphological agent. Earth-Science Reviews 74 (3-4), 269–307. doi:10.1016/j.earscirev.2005.10.006.

Smits, K.M., KIRBY, E., MASSMAN, W.J., BAGGETT, L.S., 2016. Experimental and Modeling Study of Forest Fire Effect on Soil Thermal

Conductivity. Pedosphere 26 (4), 462–473. doi:10.1016/S1002-0160(15)60057-1.

Smits, K.M., Sakaki, T., Howington, S.E., Peters, J.F., Illangasekare, T.H., 2013. Temperature Dependence of Thermal Properties of Sands across a Wide Range of Temperatures (30-70°C). Vadose zone j. 12 (1), vzj2012.0033. doi:10.2136/vzj2012.0033.

Socrates, G., 2015. Infrared and Raman characteristic group frequencies: Tables and charts, 3rd ed. ed. John Wiley & Sons LTD, Chichester [etc.], Skoroszyt.

Stauffer, F., Bayer, P., Blum, P., Giraldo, N.M., Kinzelbach, W., 2013. Thermal Use of Shallow Groundwater. CRC Press.

Tarnawski, V.R., Wagner, B., Leong, W.H., McCombie, M., Coppa, P., Bovesecchi, G., 2021. Soil thermal conductivity model by de Vries: Re-examination and validation analysis. Eur J Soil Sci 72 (5), 1940–1953. doi:10.1111/ejss.13117.

Tong, F., Jing, L., Zimmerman, R.W., 2009. An effective thermal conductivity model of geological porous media for coupled thermo-hydro-mechanical systems with multiphase flow. International Journal of Rock Mechanics and Mining Sciences 46 (8), 1358–1369. doi:10.1016/j.ijrmms.2009.04.010.

Vries, D.A. de, 1963. Thermal properties of soils. Physics of Plant Environment. https://sci-hub.st/https://ci.nii.ac.jp/naid/10016146353/.

Vries, D.A. de, Philip, J.R., 1986. Soil Heat Flux, Thermal Conductivity, and the Null-alignment Method. Soil Sci. Soc. Am. J. 50 (1), 12–18. doi:10.2136/sssaj1986.03615995005000010003x.

Wang, Z., Feyen, J., Ritsema, C.J., 1998. Susceptibility and predictability of conditions for preferential flow. Water Resour. Res. 34 (9), 2169–2182. doi:10.1029/98WR01761.

Wang, Z., Pereira, J.-M., Gan, Y., 2020. Effect of Wetting Transition during Multiphase Displacement in Porous Media. Langmuir : the ACS journal of surfaces and colloids 36 (9), 2449–2458. doi:10.1021/acs.langmuir.9b03780.

Wang, Z., Wu, L., Wu, Q., 2000. Water-entry value as an alternative indicator of soil water-repellency and wettability. Journal of Hydrology 231-232, 76–83. doi:10.1016/S0022-1694(00)00185-2.

Washburn, E.W., 1921. The Dynamics of Capillary Flow. Phys. Rev. 17 (3), 273–283. doi:10.1103/PhysRev.17.273.

Wenzel, R.N., 1936. RESISTANCE OF SOLID SURFACES TO WETTING BY WATER. Ind. Eng. Chem. 28 (8), 988–994. doi:10.1021/ie50320a024.

Wiener, O., 1912. Die Theorie des Mischkorpers fur das Feld der stationaren Stromung. Abhandlungen der Sachsischen Gesellschaft der Akademischen Wissenschaften in Mathematik und Physik 32, 507–604. https://ci.nii.ac.jp/naid/10018592156/.

Wijewardana, Senani, N., Kawamoto, K., Moldrup Per, Komatsu Toshiko, Kurukulasuriya, Chandana, L., Priyankara, H., Nadeej, 2015. Characterization of water repellency for hydrophobized grains with different geometries and sizes. Environ Earth Sci 74 (7), 5525–5539. doi:10.1007/s12665-015-4565-6.

Xiao, S., Suleiman, M.T., 2015. Investigation of Thermo-Mechanical Load Transfer (t-z Curves) Behavior of Soil-Energy Pile Interface Using Modified Borehole Shear Tests, in: IFCEE 2015. IFCEE 2015, San Antonio, Texas. March 17–21, 2015. American Society of Civil Engineers, [Place of publication not identified], pp. 1658–1667.

Young, T., 1805. III. An essay on the cohesion of fluids. Phil. Trans. R. Soc. 95, 65–87. doi:10.1098/rstl.1805.0005.

Yu, X., Zhang, N., Pradhan, A., Puppala, A.J., 2016. Thermal conductivity of sand–kaolin clay mixtures. Environmental Geotechnics 3 (4), 190–202. doi:10.1680/jenge.15.00022.

Zhang, N., Wang, Z., 2017. Review of soil thermal conductivity and predictive models. International Journal of Thermal Sciences 117, 172–183. doi:10.1016/j.ijthermalsci.2017.03.013.

Zhang, N., Yu, X., Pradhan, A., Puppala, A.J., 2017a. A new generalized soil thermal conductivity model for sand–kaolin clay mixtures using thermo-time domain reflectometry probe test. Acta Geotech. 12 (4), 739–752. doi:10.1007/s11440-016-0506-0.

Zhang, N., Yu, X., Wang, X., 2017b. Use of a thermo-TDR probe to measure sand thermal conductivity dryout curves (TCDCs) and model prediction. International Journal of Heat and Mass Transfer 115, 1054–1064. doi:10.1016/j.ijheatmasstransfer.2017.08.102.

Zhang, N., Zou, H., Zhang, L., Puppala, A.J., Liu, S., Cai, G., 2020. A unified soil thermal conductivity model based on artificial neural network. International Journal of Thermal Sciences 155, 106414. doi:10.1016/j.ijthermalsci.2020.106414.

Zheng, S., 2019. Hydrological and erosional processes in synthetic water repellent soils: HKU Theses Online (HKUTO).

Zheng, S., Xing, X., Lourenço, S.D.N., Cleall, P.J., 2021. Cover systems with synthetic water‐repellent soils. Vadose zone j. doi:10.1002/vzj2.20093.

Zhou, Y., Li, S., Zhao, Y., Ling, Z., Zhang, Z., Fang, X., 2022. Compatible paraffin@SiO2 microcapsules/polydimethylsiloxane composites with heat storage capacity and enhanced thermal conductivity for thermal management. Composites Science and Technology 218, 109192. doi:10.1016/j.compscitech.2021.109192.

Zisman, W.A., 1964. Relation of the Equilibrium Contact Angle to Liquid and Solid Constitution, in: Fowkes, F.M. (Ed.), Contact Angle, Wettability, and Adhesion, vol. 43. AMERICAN CHEMICAL SOCIETY, WASHINGTON, D.C., pp. 1–51.